Redox Biology 62 (2023) 102707

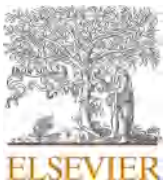

Contents lists available at ScienceDirect

Redox Biology

journal homepage: www.elsevier.com/locate/redox

The deubiquitinase USP11 ameliorates intervertebral disc degeneration by regulating oxidative stress-induced ferroptosis via deubiquitinating and stabilizing Sirt3

Jian Zhu [a,1], Ruping Sun [b,1], Kaiqiang Sun [c,1], Chen Yan [a], Jialin Jiang [a], Fanqi Kong [a,2], Jiangang Shi [a,2,*]

[a] Department of Orthopedics, Changzheng Hospital, Naval Medical University, No.415 Fengyang Road, Shanghai, 200003, China
[b] School of Health Science and Engineering, University of Shanghai for Science and Technology, No. 516 Jungong Road, Shanghai, 200093, China
[c] Department of Orthopaedic Surgery, Naval Medical Center, Naval Medical University, Shanghai, 200433, China

ARTICLE INFO

Keywords:
USP11
Sirt3
Oxidative stress-induced ferroptosis
IVDD
De-ubiquitination

ABSTRACT

Increasing studies have reported that intervertebral disc degeneration (IVDD) is the main contributor and independent risk factor for low back pain (LBP), it would be, therefore, enlightening that investigating the exact pathogenesis of IVDD and developing target-specific molecular drugs in the future. Ferroptosis is a new form of programmed cell death characterized by glutathione (GSH) depletion, and inactivation of the regulatory core of the antioxidant system (glutathione system) GPX4. The close relationship of oxidative stress and ferroptosis has been studied in various of diseases, but the crosstalk between of oxidative stress and ferroptosis has not been explored in IVDD. At the beginning of the current study, we proved that Sirt3 decreases and ferroptosis occurs after IVDD. Next, we found that knockout of Sirt3 ($Sirt3^{-/-}$) promoted IVDD and poor pain-related behavioral scores via increasing oxidative stress-induced ferroptosis. The (immunoprecipitation coupled with mass spectrometry) IP/MS and co-IP demonstrated that USP11 was identified to stabilize Sirt3 via directly binding to Sirt3 and deubiquitinating Sirt3. Overexpression of USP11 significantly ameliorate oxidative stress-induced ferroptosis, thus relieving IVDD by increasing Sirt3. Moreover, knockout of USP11 in vivo ($USP11^{-/-}$) resulted in exacerbated IVDD and poor pain-related behavioral scores, which could be reversed by overexpression of Sirt3 in intervertebral disc. In conclusion, the current study emphasized the importance of the interaction of USP11 and Sirt3 in the pathological process of IVDD via regulating oxidative stress-induced ferroptosis, and USP11-mediated oxidative stress-induced ferroptosis is identified as a promising target for treating IVDD.

1. Introduction

Low back pain (LBP) refers to pain or discomfort existing between the lumbar and sacral regions of back [1]. There is a considerable amount of LBP in the general population, 84% of the general population is likely to suffer from LBP during their lifespans [2], and according to estimates, incidence of relapse for LBP could be higher to 80% [3]. Intervertebral disc degeneration (IVDD), a common musculoskeletal degenerative disorder, is identified as the majorx cause of LBP [4], which is responsible for more than 40% of all LBP cases [5], causing significant socio-economic burdens worldwide [6]. The normal intervertebral disc is composed of three main parts: the highly-hydrated gelatinous nucleus pulposus (NP) tissue in the core, annulus fibrosus (AF) tissue circumferentially surrounding the NP tissue, and endplates (EP) tissue covering NP tissue [7,8]. With multi-pathological factors, including aging, unhealthy lifestyle, biomechanical overload and so on, the NP tissue becomes more fibrous instead of gelatinous, accompanied by decreased type II collagen and aggrecan, eventually leading to the onset and progress of IVDD [9–12]. Although there are numerous research projects focusing on the mechanisms of IVDD, its exact

* Corresponding author. Department of Orthopedic Surgery, Spine Center, Changzheng Hospital, Naval Medical University No.415 Fengyang Road, Shanghai, 200003, People's Republic of China.
E-mail address: shijiangangspine@163.com (J. Shi).
[1] Jian Zhu, Ruping Sun, and Kaiqiang Sun contributed equally to this study and should be considered as the co-first authors.
[2] Fanqi Kong and Jiangang Shi contributed equally to this study regarding the design and revision, and should be considered as co-corresponding authors.

https://doi.org/10.1016/j.redox.2023.102707
Received 2 March 2023; Received in revised form 11 April 2023; Accepted 20 April 2023
Available online 20 April 2023

pathogenesis still remains to be elucidated [13–15].

Programmed cell death (PCD) refers to an intracellular death program, which plays a vital role in maintaining biological homeostasis [16,17], and abnormal PCD has been proved to be involved in the onset and progress of various diseases [18–20]. Ferroptosis, different from autophagy, necrosis or apoptosis in morphology and pathological process, is a new form of PCD [21,22]. Ferroptosis essentially is oxidative injury caused by intracellular iron- or ester oxygenase-induced catalyzation of unsaturated fatty acids on cell membranes and lipid peroxidation, characterized by glutathione (GSH) depletion, and inactivation of the regulatory core of the antioxidant system (glutathione system) GPX4 [23,24]. Glutathione peroxidase 4 (GPX4) and ferritin heavy chain (FTH) exert anti-ferroptosis effect via catalyzing the lipid hydroperoxides and transporting intracellular iron ions, respectively [25,26]. Moreover, long-chain acyl-CoA synthetase 4 (ASL4) and prostaglandin-endoperoxide synthase 2 (PTGS2) have been proved to be involved in the activation and progression of ferroptosis, and the expressions of ACSL4 and PTGS2 are related positively with ferroptosis [27,28]. Oxidative stress is closely related to ferroptosis because of similar pathological process, and the crosstalk between of oxidative stress and ferroptosis has been studied in some diseases, including ischemic stroke and Alzheimer's disease [29,30]. However, the relevance of the crosstalk between oxidative stress and ferroptosis in IVDD has not been explored. Sirt3, a key regulator of mitochondrial reactive oxygen species (ROS), is an NAD^+-dependent mitochondrial deacetylase that promotes efficient oxidative metabolism. Sirt3 has been proved to inhibit ferroptosis in gallbladder cancer through promoting the expression of GPX4 [31,32]. However, the effect of Sirt3 on ferroptosis in IVDD has not been studied. Previous studies have showed that Sirt3 could ameliorate IVDD by suppressing senescence, inflammation and oxidative stress [33–35], which implies that stabilizing and increasing the expression of Sirt3 may be a potential therapeutic method for treating IVDD.

Protein translational modifications (PTMs) are modifications after translation intended to increase the functional diversity of the proteome through the covalent addition of a functional group or protein, the proteolytic modification of a regulatory subunit, or the degradation of the entire protein which include phosphorylation, glycosylation, ubiquitination, methylation, membrane transport and so on [36]. Deubiquitinase (DUB) mainly hydrolyzes ester, peptide or isopeptide bonds at the carboxy-terminal of ubiquitin to specifically hydrolyze ubiquitin molecules from ubiquitin linked proteins or precursor proteins, thus preventing the protein from being degraded. Whether there is a kind of DUB can stabilize Sirt3 and prevent disc degeneration has not been investigated. Ubiquitin specific protease 11 (USP11) plays a crucial role in various biological processes, including regulating cell proliferation, cancer growth and metastasis, cancer chemoresistance, and intracerebral hemorrhage [37–40]. However, the functional effect of USP11 on Sirt3 in IVDD has not been studied. In the current study, we identified USP11 as the DUB that directly deubiquitinates and stabilizes Sirt3. Notably, USP11 depletion promotes oxidative stress-induced ferroptosis by destabilizing Sirt3, leading to more severe IVDD and poor pain-related behavioral scores.

2. Methods and materials

2.1. The acquisition of human NP tissue

The current study was approved by the ethics committee of Shanghai Changzheng Hospital, Naval Medical University, and the written informed consent signed by all patients was obtained. According to the Pfirrmann grades on preoperative MRI, the NP tissues were categorized as three groups: non or slight-degeneration group (Grade I or II), medium degeneration group (Grade III), and severe degeneration group (Grade IV or V). **All experiments in the current study involving human NP samples were conform to the Helsinki declaration (World Medical Association, 2014).**

2.2. Primary human NP cells (HNP) cells and HEK 293 T cell line culture

The HNP cells were isolated in vitro from Pfirrmann Grade II patients. Briefly, the NP tissues obtained intraoperatively were transported to ultra-clean laboratory with 0.9% sodium chloride solution. After being washed 3 times with sterilized PBS (G0002, Servicebio, China), the NP tissues were digested with 0.25% Trypsin-EDTA (G4001, Servicebio, China) for half an hour, and with equal amount of collagenase type II (0.2%, Invitrogen, USA) and complete DMED/F-12 medium (contained 10% fetal bovine serum and 1% penicillin-streptomycin) for another 1 h under a shaker (37 °C, 75 rpm). After being centrifuged with 1250 rpm for 5 min, HNP were resuspended with complete DMED/F-12 medium (contained 10% fetal bovine serum and 1% penicillin-streptomycin). Subsequently, the HNP cells were counted and replanted at T25 culture flask in an aseptic atmosphere of 5% CO_2 at 37 °C. The HEK 293 T cells were purchased from QuiCell Biotechnology Co., LTD (Shanghai, China). Further experiments were available when the confluence reached to 80%. To simulate the role of oxidative stress and cell dysfunction during IVDD, cells were exposed to *tert*-butyl hydroperoxide (TBHP) at the concentration of 100 μM for 3 h, at which time TBHP media were replaced with fresh media.

2.3. Quantitative reverse transcription polymerase chain reaction analysis (qRT-PCR)

The qPCR was performed as demonstrated previously [41]. Briefly, total RNAs were extracted using Rapture Universal RNA Plus Kit (R4013-02, Magen, China) under the instructions of manufacturer. Total purified RNAs were reverse-transcribed to cDNAs, which were subsequently quantified using ChamQ Universal SYBR qPCR Master Mix (Q711-03, Vazyme, China) in StepOnePlus PCR System (Applied Biosystems, USA). The GAPDH level was used for normalization. The expression of relative gene was quantified using the $2^{-\Delta\Delta Ct}$ method and standardized as the fold of target genes to GAPDH.

2.4. Immunohistochemical (IHC) assay

Briefly, the human NP tissues embedded in paraffin were cut in 15 μm sections. Then, the sections were deparaffinized with environment-friendly de-paraffin liquid (G1128, Servicebio, China) and dehydrated using gradient alcohol. The membrane-breaking solution (G1204, Servicebio, China) was used under the protocols. The sections were subsequently incubated with 3% BSA for 25 min to block the endogenous peroxidase, then with primary antibody against Sirt3 (#AF5135, Affinity, China, 1:200), GPX4 (#DF6701, Affinity, China, 1:200), FTH (#DF6278, Affinity, China, 1:50), ADAMTS5 (#DF13268, Affinity, China, 1:150), and MMP3 (#AF0217, Affinity, China, 1:100), at 4 °C overnight. On the second day, the sections were incubated with HRP-conjugated Goat Anti-Rabbit IgG H&L (511,203, ZENBIO, China, 1:300) for 1 h, finally the counterstaining was performed with hematoxylin solution for 5 min. The images of stained sections were obtained using the light microscopy (BX43, Olympus, Japan).

2.5. Western blotting (WB) analysis

The process of WB has been demonstrated in our previous study [41]. Briefly, the total proteins of different group were extracted using whole cell lysis assay kit (KGP250/KGP2100, KeyGEN BioTech, China) under the instructions of manufacturer. BCA Protein Assay Kit was used to quantify the protein concentration and the protein solutions of the same concentration were prepared with Omni-Easy™ Protein Sample Loading Buffer (LT101S, Epizyme Biomedical Technology Co., Ltd, China). Equal amounts of total protein (80 μg) per well were separated by 10% SDS-PAGE electrophoresis. The electrophoresis was conducted at 250 V

for 30 min, then the proteins were transferred to 0.45 μm pore size PDVF membrane (IPVH00010, Millipore, USA). After being incubated with protein-free quick block solution (G2052, Servicebio, China), the proteins were incubated with primary antibodies against Sirt3(AF5135, Affinity, China, 1:1500), USP11 (R22861, ZENBIO, China, 1:800), ACSL4 (DF12141, Affinity, China, 1:1500), FTH (DF6278, Affinity, China, 1:1500), GPX4 (DF6701, Affinity, China, 1:1500), PTGS2 (66351-1-Ig, ProteinTech, China, 1:5000), ACAN (DF7561, Affinity, China, 1:1500), ADAMTS5 (DF13268, Affinity, China, 1:1500), Col2 (AF0135, Affinity, China, 1:1500), MMP3 (AF0217, Affinity, China, 1:1500), Flag (R24091, ZENBIO, China, 1:6000), Myc (343,250, ZENBIO, China, 1:800), and HA (390,001, ZENBIO, China, 1:8000), at 4 °C overnight. After washing with TBST for 3 times, the proteins were incubated with HRP-conjugated Goat Anti-Rabbit IgG H&L (511,203, ZENBIO, China, 1:3000) or Goat Anti-Mouse IgG (1:3000) for 2 h under room temperature. After washed with TBST, the immunoreactive bands were visualized and detected using Omni-ECL™ Femto Light Chemiluminescence Kit under the manufacture's instruction (SQ201L, Epizyme Biomedical Technology Co., Ltd, China), and then exposed to X-ray film and developed in Automatic chemiluminescence/-fluorescence image analysis system (5200, Tanon, China).

2.6. Immunofluorescence analysis

The HNP cells with different treatment were immunofluorescent stained for Sirt3, ACAN, and MMP3 as previously described [15]. Briefly, the samples were fixed with 4% PFA for 25 min and were penetrated for another 10 min with Triton X-100 (0.1% vol/vol), blocked subsequently with 5% BSA at room temperature for 60 min. Then the samples were incubated with relative primary antibodies at 4 °C overnight. The HNP cells were washed with cold PBS for three times, followed by incubated with a 1:500 dilution of a secondary antibody (550,076, Zen Bio, China) at room temperature for 60 min. The nuclei visualization was performed using 2-(4-amidinophenyl)-1H-indole-6-carboxamidine (DAPI). Finally, the HNP cells were sealed with the anti-fluorescence quencher (G1401, Servicebio, China) and observed under fluorescence microscope (DS-Ri2, Nikon, Japan).

2.7. Superoxide assay

Superoxide was detected using Superoxide Assay Kit (S0060, Beyotime, China) under the instructions of manufacturer. Briefly, the working solution for each detection was prepared according the proportion as follows: 200 μl superoxide detection buffer +10 μl WST-1 solution +2 μl Catalase. Added 200 μl of superoxide test solution to each well and incubated at 37 °C for 3 min. A microplate reader was used to measure the absorbance at the wave length of 450 nm.

2.8. Mitochondrial superoxide assay

MitoSOX™ red (M36008, Invitrogen, USA) was used as indicator to measure mitochondrial superoxide production. The slides of cells were dyed with 5 μM MitoSOX at incubator for 8 min away from light. Then the cells were washed gently for 3 times with warm PBS. Finally, the cells were sealed with the anti-fluorescence quencher (G1401, Servicebio, China) and observed under fluorescence microscope (Olympus, Japan).

2.9. Enzyme-linked immunosorbent (ELISA) assay

NP tissues harvested from humans or mice were cut into fine fragments and weighed, 100 mg tissue samples were harvested, added into 1 ml of the Radio Immunoprecipitation Assay lysis buffer (RIPA, PC102, Epizyme Biomedical Technology Co., Ltd, China) that contained 10 μl of protease inhibitor (GRF101, Epizyme Biomedical Technology Co., Ltd, Chin). Then the tissues were placed into high-speed tissue grinder (KZ-II, Servicebio, China) for 5 min for sufficient grinding, then subjected to centrifugation (2000 rpm for 20 min) to obtain the supernatant. ELISA kits were used for the measurement of ferric ion (G01670, Westang, China), malonaldehyde (MDA, F01963, Westang, China) arend GSH (G02170, Westang, China) under the instructions of manufacturer.

2.10. Lipid peroxidation assay

The level of lipid peroxidation, an indicator of ferroptosis, was measured using a sensor BODIPY™ 581/591 C11 (D3861; Invitrogen™) according to the instructions of manufacturer. Briefly, HNP cells were incubated with BODIPY™ 581/591 C11 (2 μM) for 1 h, then washed twice with sterilized cold PBS. Subsequently, the imaging slides were fixed with 4% paraformaldehyde and sealed with the anti-fluorescence quencher (G1401, Servicebio, China). The change of lipid peroxidation was standardized and showed by the ratio of green fluorescence to red fluorescence.

2.11. Co- immunoprecipitation (Co-IP)

The Co-IP was performed using Classic Magnetic Protein A/G IP/Co-IP Kit under the manufacturer's instruction (YJ201, Epizyme Biomedical Technology Co., Ltd, China). Briefly, the cells were firstly washed with cold PBS, then incubated with appropriate amount of immunoprecipitation lysis buffer (500 μl) containing protease inhibitor (GRF101, Epizyme Biomedical Technology Co., Ltd, China) for 10 min on ice. The centrifugation (12,000 rpm for 20 min) was performed to obtain the supernatant, a small amount of which was collected for western blotting analysis (input group). To obtain antigen-antibody-magnetic bead complex, corresponding primary antibody (10 μl) and pretreated protein A/G magnetic beads (YJ003, Epizyme Biomedical Technology Co., Ltd, China) were added to the remaining supernatant (total protein content was 1000 μg) and incubated on a turn over-mixer (15920D, Thermo Fisher Scientific, USA) at room temperature for 2 h. The antigen-antibody-magnetic bead complex was settled to the bottom of the tube under the action of the magnetic frame (XY008, Epizyme Biomedical Technology Co., Ltd, China), and was washed subsequently with lysis buffer for 4 times. The antibody-antibody-magnetic bead complex was mixed with 60 μL1 × SDS-PAGE loading buffer (LT101, Epizyme Biomedical Technology Co., Ltd, China) and heated at 100 °C for 10 min. After the magnetic beads were adsorbed on the bottom of the centrifuge tube, the supernatant was collected for further SDS-PAGE detection.

2.12. Immunoprecipitation coupled with mass spectrometry assay (IP coupled with MS/MS)

The antigen-antibody-magnetic bead complex was obtained as described above. Then the mass spectrometry (Thermo Fisher Scientific, USA) was conducted to evaluated the isolated immunoprecipitates. Briefly, about 320 μl of SDT (4%SDS, 100 mM Tris-HCl, pH7.6) buffer was used for sample lysis and protein extraction. The samples were incubated with trypsin (the wt/wt ratio of trypsin: protein was 1:50) at 37 °C overnight to obtain peptides samples. The peptides were then desalted on C18 Cartridges (Empore™ SPE Cartridges C18 (standard density), bed I.D. 7 mm, volume 3 ml, Sigma), concentrated by vacuum centrifugation and reconstituted in 40 μl of 0.1% (v/v) formic acid. The peptide content was estimated by UV light spectral density at 280 nm using an extinctions coefficient of 1.1 of 0.1% (g/l) solution. Then 1 μg of peptide sample was prepared for further LC-MS/MS analysis. LC-MS/MS analysis was performed on a Q Exactive mass spectrometer (Thermo Fisher Scientific, USA) that was coupled to Easy nLC (Thermo Fisher Scientific, USA) for 120 min. Automatic gain control (AGC) target was set to 3e6, and maximum inject time to 10 ms. Dynamic exclusion duration was 40.0 s. Survey scans were acquired at a resolution of 70,000 at m/z 200, and isolation width was 2 *m/z*. Normalized collision energy was 30 eV and the underfill ratio was defined as 0.1%. The

instrument was run with peptide recognition mode enabled. The MS raw data for each sample were combined and searched using the MaxQuant 1.5.3.17 software for identification and quantitation analysis. Cluster 3.0 (http://bonsai.hgc.jp/~mdehoon/software/cluster/software.htm) were used to performing hierarchical clustering analysis.

2.13. Construction of gene knockout mice

The gene knockout mice were constructed using CRISPR/Cas9. Sirt3$^{-/-}$ mice were maintained and bred as described previously [42]. Briefly, Sirt3 is located on chromosome 7 of mice. CRISPR/Cas9 technology was used to obtain Sirt3 gene knockout mice (C57BL/6 N) by applying high-throughput electro-transfer to fertilized eggs. USP11$^{-/-}$ mice were generated from Cyagen Biosciences Inc. In brief, the USP11 gene (NCBI Reference Sequence: NM_145628.4) was located on chromosome X of mouse, from which 21 exons were identified, with the start codon (ATG) in exon 1 and the stop codon (TAA) in exon 21. Exon 2~ exon 9 was selected as target site. Cas9 coupled with gRNA (gRNA-A1-TTTAGTTGTGCAGGATGGCGGGG,
gRNA-A2-GGCTACCCATTAAAGCTACATGG) were co-injected in fertilized eggs for generating USP11–KO mice. The pups were genotyped by PCR, followed by sequencing analysis.

2.14. Construction of a mouse model of IVDD

The mouse model of IVDD was established through constructing lumbar spine instability (LSI). The current study was approved by the Ethics Committee of Naval Medical University. All procedures involving animal experiments were in accordance with the guidelines of The Animal Research: Reporting of in vivo Experiments (ARRIVE). Briefly, 8–10 weeks old male mice were placed in prone position and anesthetized with isoflurane inhalation. The 1.5 cm-long longitudinal incision was made in 2 mm from the posterior midline. The superior and inferior articular processes, supraspinous ligament and interspinous ligament of the L4–L5 lumbar vertebrae were removed to construct LSI, which would induce IVDD. After the operation, the mice were placed in a warm environment.

2.15. Behavioral testing

Four kinds of pain-related behavioral test were performed. Vocalization thresholds that indicate pressure hyperalgesia were conducted using a force gauge (Bioseb, USA), the mice restrained by sensor tip were pressed at skin over L4/5 with increasing force at 50 g/s until the mice made a vocalization. Three indexes of spontaneous activity of mice (including distance walked, total active time, and maximum speed) were evaluated by using wheel activity device (Bioseb, USA) that could be spun by mice in both directions, were recorded in the current study.

2.16. Hematoxylin and Eosin (H&E), and safranin O & Fast Green (S&F) staining

Briefly, the mice NP tissues embedded in paraffin were cut in 15 μm sections. Subsequently, the sections were deparaffinized with environment-friendly de-paraffin liquid (G1128, Servicebio, China) and dehydrated using gradient alcohol. The sections were stained with Hematoxylin and Eosin, or with Safranin O and Fast Green under the instructions of protocol. The images of stained sections were obtained using the light microscopy (Olympus, Japan).

2.17. Small interfering RNA (siRNA) transfection

USP11-siRNA and Sirt3-siRNA were purchased from GenePharma Biotechnology Co., LTD (Shanghai, China). The sequences were listed as follows: siRNA-USP11-1 (sense sequence: 5′-GAUGGUUAAUGUUAUGUUAUG-3′, antisense sequence: 5′-UAACAUAACAUUAACCAUCUU-3′), siRNA-USP11-2 (sense sequence: 5′- GGAUAUAUGUGUUUAUAAAGC-3′, antisense sequence: 5′- UUUAUAAACACAUAUAUCCUG-3′), siRNA-Sirt3 (sense sequence: 5′-GGAUGUAGCUGAGCUGAUUCG-3′, antisense sequence: 5′- AAUCAGCUCAGCUACAUCCUG-3′). Then the siRNAs were transfected into human NP cells by using Lipo8000™ reagent (C0533, Beyotime, China) while si-Ctrl was used as a negative control.

2.18. Transmission electron microscopy for NP cells

When the cell confluence reached 80%, the complete medium was discarded and the cells were washed with cold PBS for four times. The cells were then digested with 0.25% trypsin (G4001, Servicebio, China) for 5 min, followed by centrifugation with 1200 rpm for 10 min. The cell pellet was fixed with 2.5% glutaraldehyde (G1102, Servicebio, China), then dehydrated with gradient ethanol for 20 min and two times of acetone for 15 min. Epoxy resin penetration and embedding as followed: acetone: epoxy resin = 1:1 for 2–4 h at 37 °C; acetone: epoxy resin = 1:2 overnight at 37 °C. Pour the pure epoxy resin into the embedding models and insert the tissues into the pure epoxy resin, and then keep in 37 °C oven overnight to establish embedding model. Polymerization was then performed as followed: The embedding models with epoxy resin and samples were moved into 65 °C oven to polymerize for more than 48 h. And then the epoxy resin blocks were taken out from the embedding models for standby application at room temperature. Subsequently, ultrathin section (75 nm thin) was performed on the ultra microtome, followed by staining with 2% uranium acetate saturated alcohol solution for 8 min away from light and 2.6% lead citrate solution for 8 min with carbon dioxide avoidance. The sections were observed under an electron microscope (HT7800, HITACHI, Japan).

2.19. Plasmids transfection

Human Flag-USP11, Flag-USP11-C318S, HA-ubiquitin (Ub) and HA-Ub mutants were purchased from Addgene (MA, USA). The protein information of USP11 (UniProt ID: P51784) and Sirt3 (UniProt ID: Q9NTG7) was acquired from UniProt website (https://www.uniprot.org/). Then the coding sequence (CDS) of USP11 (GenBank ID: BC140849.1) and Sirt3 (GenBank ID: AF083108.2) was obtained from National Center for Biotechnology Information (https://www.ncbi.nlm.nih.gov/). The full-length sequence or different domain sequences of USP11 and Sirt3 were synthesized and subcloned into Flag-, or Myc-tagged pEX-3 (pGCMV/MCS/Neo) vectors by GenePharma Biotechnology Co., LTD (Shanghai, China). Human NP cells or Human embryonic kidney T cells (HEK 293 T cells, purchased from QuickCell, China) were transfected with above plasmid using Lipo8000™ reagent (C0533, Beyotime, China). Briefly, the day before transfection, the cells were seeded in 6-well plates (about 5×10^4 cells per well). The culture medium was changed when the cells reached 80% confluence. Added the mixture with the amount of 130 μl (125 μl of Opti-MEM + 2.5 μg of DNA + 4 μl of Lipo8000™ reagent) into each well, and incubated for 24 h.

2.20. Adeno-associated virus (AAV) infection

To increase the in vivo expression of USP11, pNeu5Aca-2-3GaINAcβ-4GlcNAc -USP11 (AAV-USP11) was used (WZ Bio Inc, China), and pNeu5Aca-2-3GaINAcβ-4GlcNAc-Ctrl (AAV-Ctrl) was selected as control vector (WZ Bio Inc, China). The viral vectors (5×10^{10} viral genome, 0.5 μl) were injected slowly into intervertebral disc using micro-injection syringe immediately after the construction of LSI model.

2.21. Magnetic resonance imaging for mice

MRI experiments for in vivo mice imaging of spine were performed on a 7.0 T MRI system designed for small animals (Bruker BioSpec 16 US/Pharmascan, Germany). Among the sequences included in this

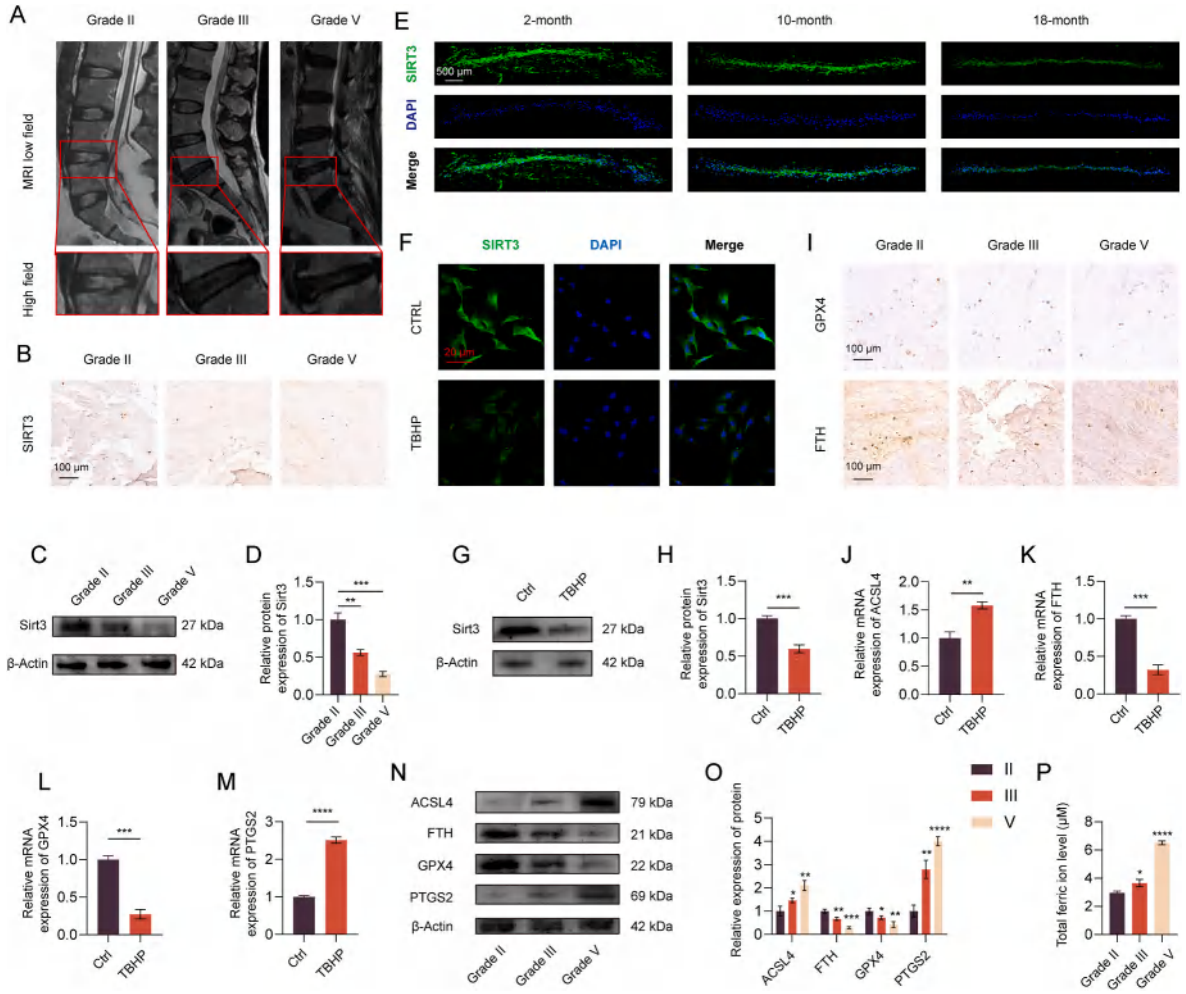

Fig. 1. (A) Magnetic resonance imaging of patients with different levels of IVDD according to Pfirrmann grades. (B) The results of IHC for human NP tissue sections demonstrated that the expression of Sirt3 was decreased with the progression of degeneration. (C, D) The expression change of Sirt3 in IVDD was further confirmed by western blotting assay, which was accordance with the result of IHC. (E). The IF for mouse intervertebral disc tissue sections proved the down-regulated Sirt3 after IVDD. (F) The expression of Sirt3 was lower in HNP cells treated with TBHP. (G, H) The administration of TBHP for HNP cells made the Sirt3 expression dropped significantly compared with control group. (I) IHC results demonstrated the lower expression of GPX4 and FTH after IVDD. (J–M) The results of qPCR proved that the expression of ACSL4 and PTGS2 was enhanced while GPX4 and FTH was decreased after IVDD. (N, O) The result of WB further confirmed the above results. (P) ELISA proved that the ferric ion increased with the progression of IVDD. * for $p < 0:05$, ** for $p < 0:01$, ***for $p < 0:001$, **** for $p < 0:0001$.

protocol are a T1-weighted sequence, a proton density-weighted sequence, a FLAIR sequence, and a T2-weighted gradient echo sequence with echo time/repetition time 27/3000 ms. Analysis and assessment for T2-weighted images in the sagittal and axial planes were undertaken using RadiAnt DICOM Viewer (V4.6.9, Medxant, Poznan, Poland). The measurement of intervertebral disc with hypointense signal was manually traced by a blinded investigator.

2.22. Statistical analysis

All experiments in the current study were performed independently for at least three times. Statistical analysis was performed using the Statistical Package for the Social Sciences (SPSS) version 26.0 (IBM Armonls, NY, USA). Continuous variables were recorded as mean values ± standard deviation (SD), and categorical variables were expressed by proportions (%). The unpaired 2-tailed Student *t*-test or Mann-Whitney *U* test were performed to compare the mean values or data distribution of continuous variables. And categorical variables were compared with the $\chi 2$ (chi-square) test or Fisher exact test, as appropriate. A P value of <0.05 was considered statistically significant.

3. Results

3.1. The expression of Sirt3 decreases and ferroptosis occurs after IVDD

To investigate the change of Sirt3 expression, NP tissues were harvested from patients with different levels of IVDD that based on the Pfirrmann grades (Fig. 1A). The result of IHC for human NP tissues demonstrated that Sirt3 expression was decreased with the progression of IVDD (Fig. 1B). The change of Sirt3 in IVDD was further proved by WB, as shown in Fig. 1C and D, the WB and standardized results were in accordance with above IHC results. Furthermore, the change of Sirt3 expression was tested on IVDD mouse model. The IF for mouse intervertebral disc tissue sections proved the down-regulated Sirt3 after IVDD (Fig. 1E), which was quantified in Fig. S1A. The mRNA expression of Sirt3 decreased significantly after exposure to TBHP in HNP cells (Fig. S1C). Fig. 1F also showed that the administration of TBHP for HNP cells made the Sirt3 expression dropped significantly compared with control group, the quantification of which was showed in Fig. S1B. Moreover, the WB showed the similar trends (Fig. 1G and H). Next, whether ferroptosis was involved in the process of IVDD was investigated. IHC results demonstrated the lower expression of GPX4 and FTH after IVDD (Fig. 1I). The results of qPCR proved that the expression of

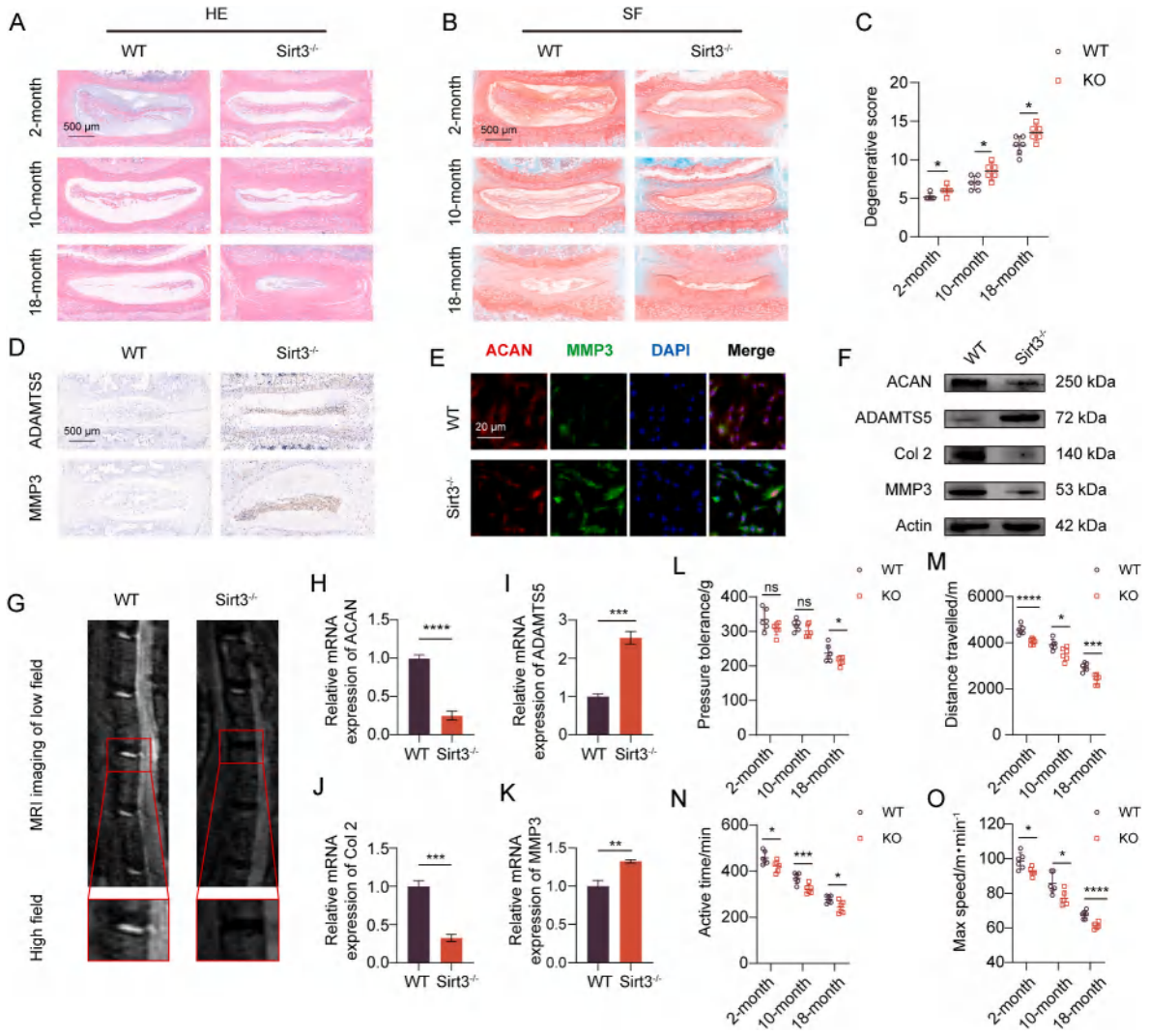

Fig. 2. (A) HE staining showed the morphology of mice discs, more severe rupture between the annulus fibrosus and nucleus pulposus was observed in Sirt3$^{-/-}$ group. (B) SF staining proved that KO of Sirt3 was associated with more severe IVDD with internuclear fibrosis. (C) Histological grades were calculated based on HE staining and SF staining results. (D) IHC results revealed that higher expression of ADAMTS5 and MMP3 in Sirt3−/− group after 6 months from the construction of IVDD model was confirmed. (E) The co-immunofluorescence of ACAN and MMP3 for HNP cells indicated that KO of Sirt3 promoted higher expression of ACAN and lower expression of MMP3. (F) Enhanced expression of ADAMTS5 and MMP3 and down-regulated expression of ACAN and Col2 was observed in WB results. (G) Reduced signal intensity was observed in Sirt3$^{-/-}$ group, which proved that KO of Sirt3 leaded to more severe IVDD. (H–K) The qPCR results accorded with the results above. (L–O) Pain-related behavioral scores, including pressure tolerance, distance walked, total active time and maximum speed, were significantly compromised in Sirt3−/− group with increasing IVDD duration. * for $p < 0:05$, ** for $p < 0:01$, ***for $p < 0:001$, **** for $p < 0:0001$, ns for no significance.

ACSL4 and PTGS2 was enhanced while GPX4 and FTH was decreased after IVDD (Fig. 1J–M). The WB further confirmed the above results (Fig. 1N, O). Total ferric ion was increased with statistical significance after IVDD, proved by ELISA (Fig. 1P).

3.2. KO of Sirt3 promotes IVDD and poor pain-related behavioral scores

We further explored the effect of KO of Sirt3 on LSI-induced IVDD via the examination of changes in morphology. The results of HE and SF, along with the degenerative scores, proved that KO of Sirt3 promotes IVDD compared with WT group (Fig. 2A–C). Extracellular matrix (ECM) degeneration, one of the characteristics of IVDD, was subsequently tested. As shown in Fig. 2D, higher expression of ADAMTS5 and MMP3 in Sirt3$^{-/-}$ group after 6 months from the construction of IVDD model was confirmed. The co-immunofluorescence of ACAN and MMP3 for HNP cells indicated that KO of Sirt3 promoted higher expression of ACAN and lower expression of MMP3 (Fig. 2E), the quantification graph of which was showed in Fig. S1D. The results of WB demonstrated that KO of Sirt3 was associated with enhanced expression of ADAMTS5 and MMP3 and down-regulated expression of ACAN and Col2 (Fig. 2F). Moreover, the MRI imaging of mouse lumbar spine showed that KO of Sirt3 resulted in more severe of IVDD (Fig. 2G). The qPCR results accorded with the results above (Fig. 2H–K). Pain-related behavioral scores, including pressure tolerance, distance walked, total active time and maximum speed, were significantly compromised in Sirt3$^{-/-}$ group with increasing IVDD duration (Fig. 2L–O). Collectively, the results above revealed that KO of Sirt3 promotes IVDD and poor pain-related behavioral scores.

3.3. KO of Sirt3 increases the oxidative stress-induced ferroptosis

Previous studies have proved that TBHP was a potent activator of oxidative stress injury [43]. The effect of KO of Sirt3 on oxidative stress was investigated in vitro based on different treatment of NP cells (Fig. 3B). As expected, the anti-oxidative stress genes, including HO-1, NQO1, SOD2 and SLC7A11, were down-regulated after the

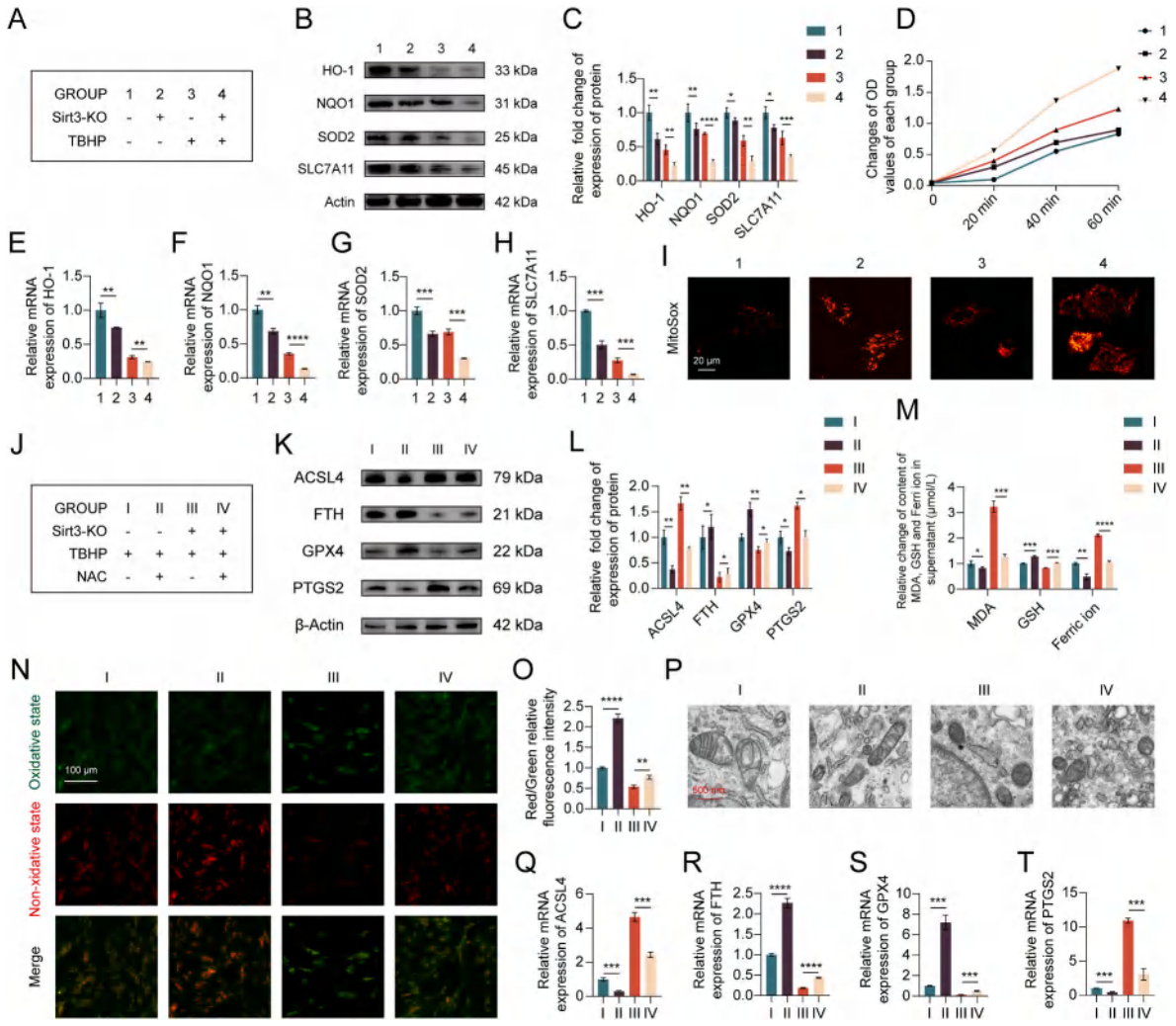

Fig. 3. (A) Detailed information of the experimental group in the part of the experiment involving oxidative stress. (B, C) KO of Sirt3 could significantly decrease the expression of anti-oxidative stress genes (HO-1, NQO1, SOD2 and SCC7A11). (D) The superoxide was increased with increasing time of TBHP treatment, and higher superoxide was observed in Sirt3-KO group at each time point. (E–H) The above result was further confirmed by qPCR. (I) Mitochondrial superoxide was up-regulated after the treatment of TBHP, which was exacerbated by KO of Sirt3. (J) Detailed information of the experimental group in investigating the effect of KO of Sirt3 on oxidative stress-induced ferroptosis. (K, L) The WB result revealed that the expression of anti-ferroptosis genes (GPX4 and FTH) were decreased while pro-ferroptosis genes (PTGS2 and ACSL4) was increased in NP cells after treated with TBHP, the deletion of Sirt3 exacerbated ferroptosis induced by oxidative stress, which could be reversed by specific oxidative stress inhibitor NAC. (M) As shown in the result of ELISA, the content of MDA and ferric ion was increased significantly in Sirt3$^{-/-}$, while GSH was dropped. (N, O) Non-peroxidative state shows red fluorescence, while peroxidative state shows green fluorescence in BODIPY assay. The result suggested that the level of lipid peroxidation was the most up-regulated in Sirt3 KO group after exposed to TBHP. (P) Mitochondrial morphology changed the most in Sirt3 KO accompanied with administration of TBHP, which was reversed partly by NAC. (Q–T) The result of qPCR was in accordance with the above results. * for $p < 0:05$, ** for $p < 0:01$, ***for $p < 0:001$, **** for $p < 0:0001$. (For interpretation of the references to colour in this figure legend, the reader is referred to the Web version of this article.)

administration of TBHP with concentration of 100 μM, which would be exacerbated by KO of Sirt3 (Fig. 3B). The results of quantified WB were presented in Fig. 3C. The superoxide was increased with increasing time of TBHP treatment, and higher superoxide was observed in Sirt3-KO group at each time point (Fig. 3D). The results above were further proved by qPCR analysis (Fig. 3E–H). Mitochondrial superoxide production was further investigated using MitoSOX. As shown in Fig. 3I, superoxide was up-regulated after the treatment of TBHP, which was exacerbated by Sirt3 KO, and fluorescence intensity was subsequently quantified (Fig. S1E). The effect of KO of Sirt3 on oxidative stress-induced ferroptosis was tested subsequently (Fig. 3J). The WB result revealed that the expression of GPX4 and FTH was decreased while PTGS2 and ACSL4 was increased after treated with TBHP, the deletion of Sirt3 exacerbated ferroptosis induced by oxidative stress, which could be reversed by specific oxidative stress inhibitor N-Acetyl-L-cysteine ethyl ester with concentration of 10 mM (Fig. 3K L). The ELISA result proved that the ferroptosis was improved in NAC-pretreated group compared with TBHP group, which revealed that the ferroptosis was induced by oxidative stress (Fig. 3M). The result of BODIPY assay suggested that the level of lipid peroxidation was the most up-regulated in Sirt3 KO group after exposed to TBHP (Fig. 3N, O). The TEM results proved that mitochondrial morphology changed the most in Sirt3 KO accompanied with administration of TBHP, which was reversed partly by NAC (Fig. 3P). The qPCR results showed the same trend (Fig. 3Q– T). Conclusively, KO of Sirt3 increased the oxidative stress-induced ferroptosis in vitro.

3.4. *USP11 interacts with Sirt3*

To investigate the mechanism through which the Sirt3 was regulated in the process of oxidative stress-induced ferroptosis, the IP/MS was used to study which proteins bind Sirt3. The result of IP/MS

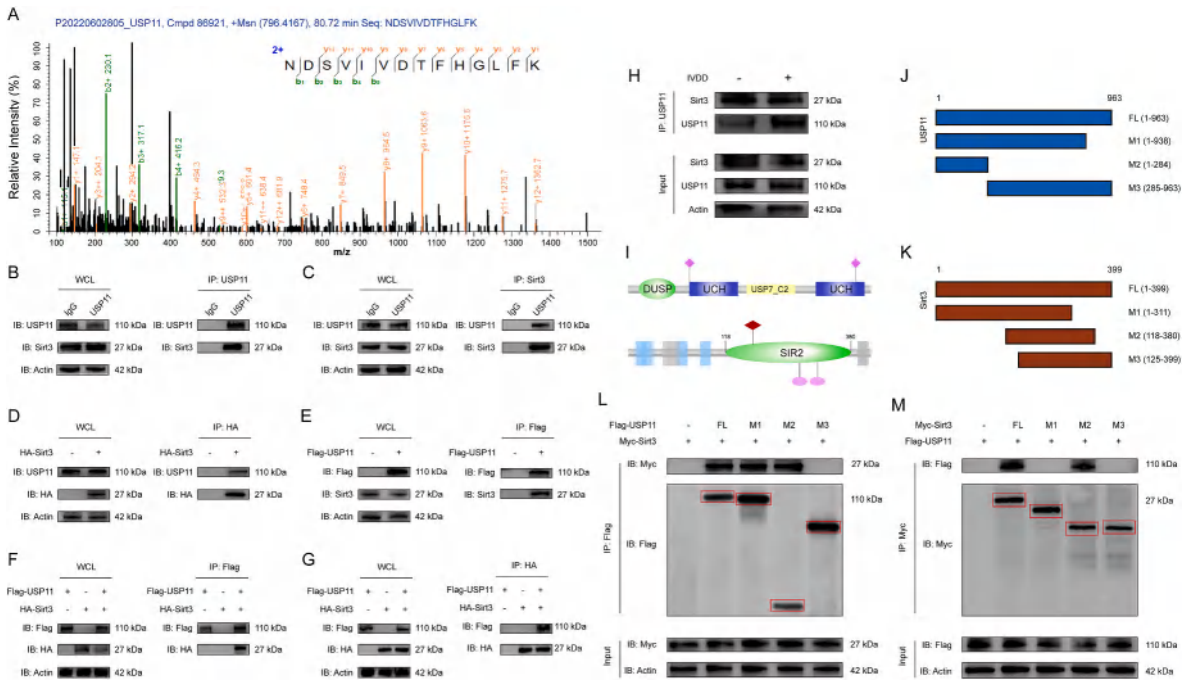

Fig. 4. (A) The result of IP/MS demonstrated that USP11 was identified to be a putative protein binding to Sirt3. To further confirm the result of IP/MS, Co-IP analysis was conducted subsequently. (B) USP11 precipitated Sirt3 in NP cells, confirming the interaction of USP11 and Sirt3. (C) Reverse Co-IP revealed that USP11 was precipitated by Sirt3 in HP cells. The Co-IP analysis using epitope-tagged proteins was further performed. (D, E) the Co-IP test with exogenous Flag-tagged USP11, or Myc-tagged Sirt3 in HEK 293 T cells could precipitate endogenous Sirt3 or USP11, respectively. (F, G) Exogenous Flag-tagged USP11 and Myc-tagged Sirt3 could co-precipitate each other efficiently in HEK 293 T cells. (H) The data above proved the interactions of USP11 and Sirt3, which could be enhanced after IVDD. (I) The schematic diagram showed that USP11 and Sirt3 contains several domains. (J, K) Full length or truncated segments of Flag-USP11 and Myc-Sirt3 containing different domains were transfected in HEK 293 T cells to investigate the binding region. (L) The Co-IP revealed that the fragment containing DUSP domain of USP11 was able to bind Sirt3. (M) Reverse Co-IP proved that USP11 interacted with M2 domain of Sirt3.

demonstrated that USP11 was identified to be a putative protein binding to Sirt3 (Fig. 4A). The interaction of USP11 and Sirt3 was further confirmed using Co-IP analysis. As presented, USP11, instead of control IgG, precipitated Sirt3 in HNP cells (Fig. 4B). Moreover, reverse Co-IP revealed that USP11 was precipitated significantly by Sirt3 in HNP cells (Fig. 4C). The Co-IP test with exogenous Flag-tagged USP11, or Myc-tagged Sirt3 in HEK 293 T cells was performed to precipitate endogenous Sirt3 or USP11, respectively (Fig. 4D and E). Further, the HEK 283 T cells were transfected with Flag-tagged USP11 and Myc-tagged Sirt3 for co-immunoprecipitation, and as expected, two exogenous tagged proteins were co-precipitated efficiently in HEK 293 T cells (Fig. 4F and G). The data above proved the interactions of USP11 and Sirt3, which could be enhanced after IVDD (Fig. 4H). To investigate the binding region, full length or truncated segments of Flag-USP11 and Myc-Sirt3 containing different domains were used (Fig. 4I–K). We proved that fragment containing DUSP domain of USP11 was able to bind Sirt3 (Fig. 4L). Reverse Co-IP demonstrated that USP11 interacted with M2 domain of Sirt3 (Fig. 4M). Collectively, the results above proved that USP11 interacts with Sirt3, and the interaction depended on the M2 domain of USP11 and M2 domain of Sirt3.

3.5. *USP11 inhibits Sirt3 ubiquitination and degradation*

The expression of Sirt3 declined spontaneously with time, which could be reversed by proteasome specific inhibitor MG132 (Fig. 5A). Next, the effect of knockdown of USP11 using siRNA on the expression of Sirt3 in HNP cells was studied. The expression of Sirt3 dropped significantly at protein level in siRNA-USP11 group compared with siRNA-Ctrl group (Fig, 5 B). On the contrary, overexpression of USP11 stabilized the expression of Sirt3 (Fig. 5C). The results above were confirmed again in HEK 293 T cells (Fig. 5D). Next, wild-type USP11 or $USP1^{C318S}$ mutant (C318S) were transfected into cells. Previous studies have proved that C318S mutant could catalytically inactive USP11 [44–46]. In accordance with previous studies, we found that overexpression of normal USP11 could upregulate the Sirt3 expression, while overexpression of USP11 with C318S mutant did not (Fig. 5E and F). Subsequently, we sought to determine that USP11 may deubiquitinate Sirt3, thus stabilize the expression of Sirt3. The ubiquitination of Sirt3 was increased effectively by knockdown of USP11, while Sirt3 decreased at protein level (Fig. 5G). To confirm the deubiquitinate effect of USP11 on Sirt3, HEK 293 T cells were transfected with plasmid of Flag-USP11, Myc-Sirt3 and HA-Ub. The results demonstrated that the deubiquitinate effect of USP11 on Sirt3 was proved (Fig. 5H). However, the de-ubiquitination of Sirt3 was abolished in IVD in $USP11^{-/-}$ mice compared with wild mice (Fig. 5I), but higher de-ubiquitination of Sirt3 and higher expression of Sirt3 was observed after IVDD in mice injected with AAV-USP11 (Fig. 5J). Next, to investigated the effect of USP11 on polyubiquitin modification of Sirt3, we mutated lysine residues at different sites of Ub to arginine (K27R, K48R or K63R) according to previous studies [47–49]. Then the HEK 293 T cells were transfected with Flag-USP11, Myc-Sirt3, and HA-Ub (wild type) or HA-Ub with mutations, from which we found that USP11 could cleave the Lys48-polyubiquitin chain instead of Lys-27 or Lys63-polyubiquitin chain (Fig. 5K). Subsequently, the K27only (a K27-only ubiquitin expression plasmid, where all lysines in ubiquitin except K27 were mutated to arginine), K48only (a K48-only ubiquitin expression plasmid, where all lysines in ubiquitin except K48 were mutated to arginine) and K63only (a K63-only ubiquitin expression plasmid, where all lysines in ubiquitin except K63 were mutated to arginine) form of HA-tagged ubiquitin were transfected into HEK 293 T cells [50–52], and we found that all forms except for K48R form of HA-tagged Ub could not be cleaved by Flag-USP11 (Fig. 5L), which revealing that Lys48-linked poly-ubiquitination was necessary for de-ubiquitination of Sirt3 regulated by USP11. Taken together, the data above confirmed that USP11

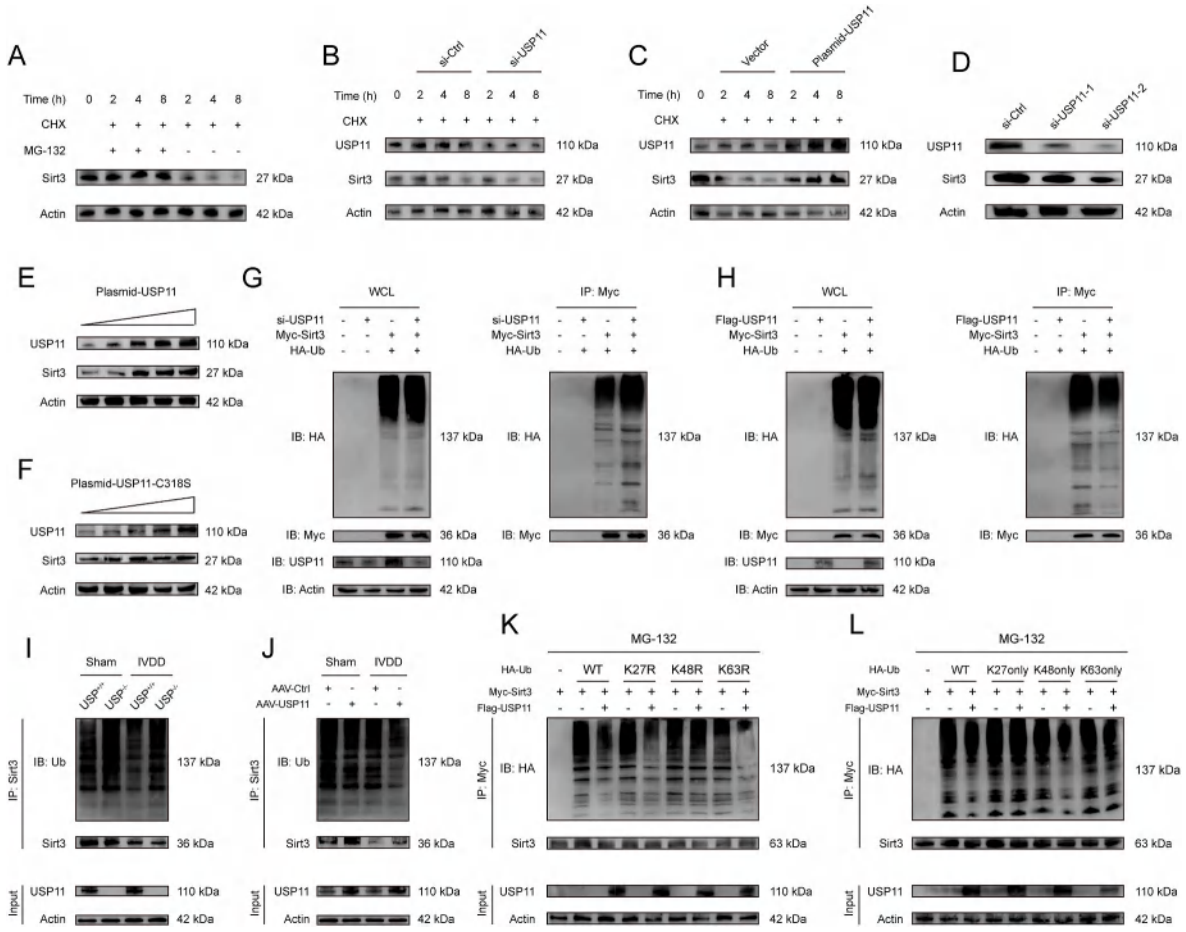

Fig. 5. (A) The expression of Sirt3 declined spontaneously with time in the presence of protein synthesis inhibitor cycloheximide (CHX, 10 μg/ml), which could be reversed by proteasome specific inhibitor MG132. Next, siRNA-USP11 or siRNA-Ctrl was transfected into HNP cells and the expression of Sirt3 was analyzed using immunoblotting. (B) The expression of Sirt3 dropped significantly after knockdown of USP11. (C) On the contrary, overexpression of USP11 stabilized the expression of Sirt3. (D) The results above were confirmed again in HEK 293 T cells. (E, F) Overexpression of normal USP11 could upregulate the Sirt3 expression, while overexpression of USP11 with C318S mutant did not. (G) The de-ubiquitination of Sirt3 was abolished effectively by knockdown of USP11. (H) HEK 293 T cells were co-transfected with plasmid of Flag-USP11, Myc-Sirt3 and HA-Ub. The results demonstrated that the deubiquitinate effect of USP11 on Sirt3 was proved. (I) The de-ubiquitination of Sirt3 was abolished in IVD in USP11$^{-/-}$ mice compared with wild mice. (J) Higher de-ubiquitination of Sirt3 and higher expression of Sirt3 was observed after IVDD in mice injected with AAV-USP11. (K) USP11 could cleave the Lys48-polyubiquitin chain instead of Lys63-polyubiquitin chain. (L). Lys48-linked poly-ubiquitination was necessary for de-ubiquitination of Sirt3 regulated by USP11.

inhibits Sirt3 degradation through deubiquitinating Sirt3.

3.6. *USP11 ameliorates ferroptosis, thus relieving IVDD by increasing Sirt3*

To confirm the regulatory effect of USP11 on ferroptosis in the process of IVDD via enhancing the expression of Sirt3, plasmid-USP11 (or plasmid-Ctrl) and siRNA-Sirt3 (or siRNA-Ctrl) were transfected into mice NP cells (Fig. 6A). WB results indicated that ferroptosis events were exacerbated by knockdown of Sirt3, including increased expression of ACSL4 and PTGS2, and decreased expression of GPX4 and FTH (Fig. 6B and C), while overexpression of USP11 could ameliorate ferroptosis events. As demonstrated in ELISA, contents of MDA and ferric ion in supernatant were surged significantly, but GSH dropped with statistical significance in siRNA-Sirt3 group, which could be reversed by co-transfected with plasmid-USP11 (Fig. 6D). The results of qPCR for ferroptosis-related genes showed the same trend (Fig. 6E–H). Interestingly, after plasmid-USP11 treatment, the morphology of mitochondria maintained well, whereas pretreatment with siRNA-Sirt3resulted in a significant decrease in mitochondrial cristae (Fig. 6I). In addition, as shown in the result of BODIPY assay, the treatment with siRNA-Sirt3 resulted in enhanced expression of lipid peroxidation, which was reversed partly by plasmid-USP11 (Fig. 6J), the quantification of BODIPY assay was showed in Fig. S1F. Moreover, it was proved that siRNA-Sirt3 resulted in enhanced expressions of ADAMTS5 and MMP3 and down-regulated expressions of ACAN and Col2, while plasmid-USP11 could mitigate IVDD (Fig. 6K L). The results above were further confirmed using qPCR (Fig. 6M– P). Collectively, this part data confirmed that USP11 could ameliorate ferroptosis and mitigate IVDD by increasing Sirt3.

3.7. *Sirt3 improves in vivo IVDD and poor pain-related behavioral scores induced by KO of USP11*

The results above confirmed that USP11 could stabilize Sirt3, thereby inhibit ferroptosis and improve pain-related behavioral scores in vitro, the in vivo experiments were then performed using KO of USP11 mice. The AAV-Sirt3 or corresponding controls were injected into IVD in USP11$^{-/-}$ mice or WT mice to generate mice with IVD-specific Sirt3 overexpression (Fig. 7A). The histological studies, including HE and SF staining, demonstrated that the boundary between AF and NP was disrupted severely, and NP cells decreased severely without vacuoles in USP11$^{-/-}$ group, which indicated that KO of USP11 resulted in more severe IVDD compared with WT group. However, the IVDD induced by

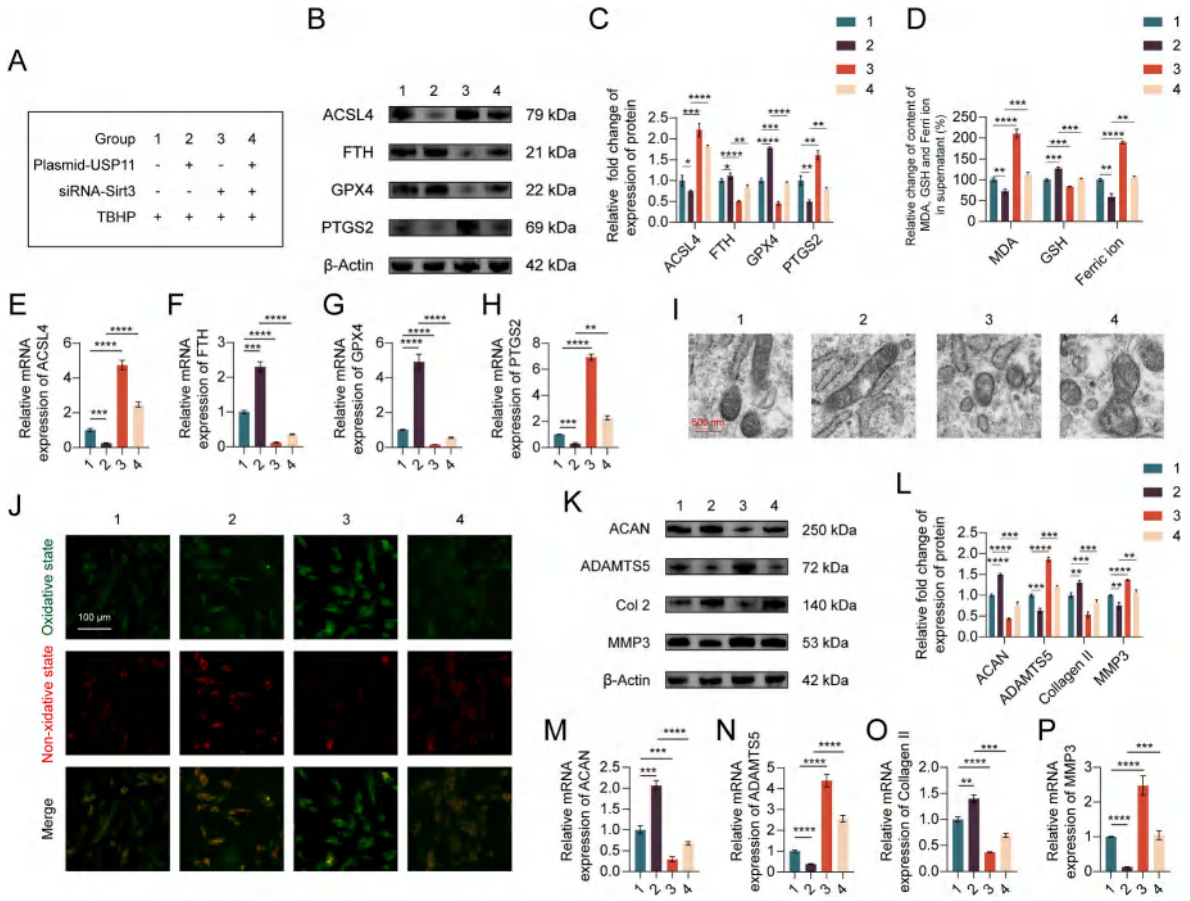

Fig. 6. (A) Detailed information of the experimental group in the part of the experiment. (B, C) Ferroptosis events were exacerbated by knockdown of Sirt3, including increased expression of ACSL4 and PTGS2, and decreased expression of GPX4 and FTH, which could be ameliorated by overexpression of USP11. (D) ELISA revealed that contents of MDA and ferric ion in supernatant were surged significantly, but GSH dropped with statistical significance in siRNA-Sirt3 group, which could be reversed by co-transfected with plasmid-USP11. (E–H) The results of qPCR for ferroptosis-related genes showed the same trend. (I) After plasmid-USP11 treatment, the morphology of mitochondria maintained well, whereas pretreatment with siRNA-Sirt3resulted in a significant decrease in mitochondrial cristae. (J) The feature of BODIPY assay is that the higher the green fluorescence intensity, the higher the lipid peroxidation level. Thus, as presented, the level of lipid peroxidation was much higher after the treatment of siRNA-Sirt3, which was reversed partly by plasmid-USP11. (K, L) WB proved that siRNA-Sirt3 resulted in enhanced expressions of ADAMTS5 and MMP3 and down-regulated expressions of ACAN and Col2, while plasmid-USP11 could mitigate IVDD. (M – P) The results above were further confirmed using qPCR. * for $p < 0:05$, ** for $p < 0:01$, ***for $p < 0:001$, **** for $p < 0:0001$. (For interpretation of the references to colour in this figure legend, the reader is referred to the Web version of this article.)

KO of USP11 could be reversed by the overexpression of Sirt3 (Fig. 7B and C). IHC results revealed that ADAMTS5 and MMP3 were increased significantly after KO of USP11, while AAV-Sirt3 could improve IVDD both in WT and USP11$^{-/-}$ mice (Fig. 7D). In addition, as shown in IF, KO of USP11 resulted in increased expression of MMP3 (green fluorescence) and decreased expression of ACAN (red fluorescence), which was reversed partly by AAV-Sirt3 (Fig. 7E), the quantification of fluorescence intensity further confirmed the result above (Fig. S1G). WB further confirmed the protective effect of AAV-Sirt3 on IVDD induced by KO of USP11 (Fig. 7F and G). The qPCR results showed the same trends (Fig. 7H–K). In addition, KO of USP11 resulting in poor pain-related behavioral scores was proved, which, however, could be improved by AAV-Sirt3 (Fig. 7L–O). In summary, these data indicated that Sirt3 inhibits IVDD induced by deletion of USP11, thus improving pain-related behavioral scores in vivo.

4. Discussion

In the current study, we proved that Sirt3 decrease and ferroptosis occurs after IVDD. KO of Sirt3 promoted IVDD and poor pain-related behavioral scores via promoting oxidative stress-induced ferroptosis. Therefore, we assumed that stabilizing and increasing the expression of Sirt3 may be a potential therapeutic method for treating IVDD. Next, we proved that USP11 could deubiquinate Sirt3 thus stabilize Sirt3. In addition, the loss-and-gain of function method was used to confirm that USP11 inhibits oxidative stress-induced ferroptosis via deubiquinating and stabilizing Sirt3, and ultimately mitigates IVDD and pain-related behavioral scores, which was reported for the first time. Therefore, we believe that USP11 may be an available therapeutic target for treating IVDD.

Increasing studies have reported that IVDD is the main contributor and independent risk factor for LBP, it would be, therefore, enlightening that investigating the exact pathogenesis of IVDD and developing target-specific molecular drugs in the future. Although there are amounts of research projects focusing on the pathogenesis of IVDD, its exact mechanism still remains to be elucidated [6,53]. Researches have proved that IVDD is a musculoskeletal degenerative disorder involving multifactorial pathogenesis, such as trauma, biomechanical change, oxidative stress, inflammatory factors, and genetic susceptibility [15,54,55]. Previous studies have reported that oxidative stress acts as an activator of autophagy, cell senescence, apoptosis, aberrant ECM metabolism, all of which could induce mitochondrial dysfunction that is responsible for the excessive production of mitochondrial ROS [56–59]. Sirt3, a key regulator of mitochondrial ROS, is an NAD^+-dependent

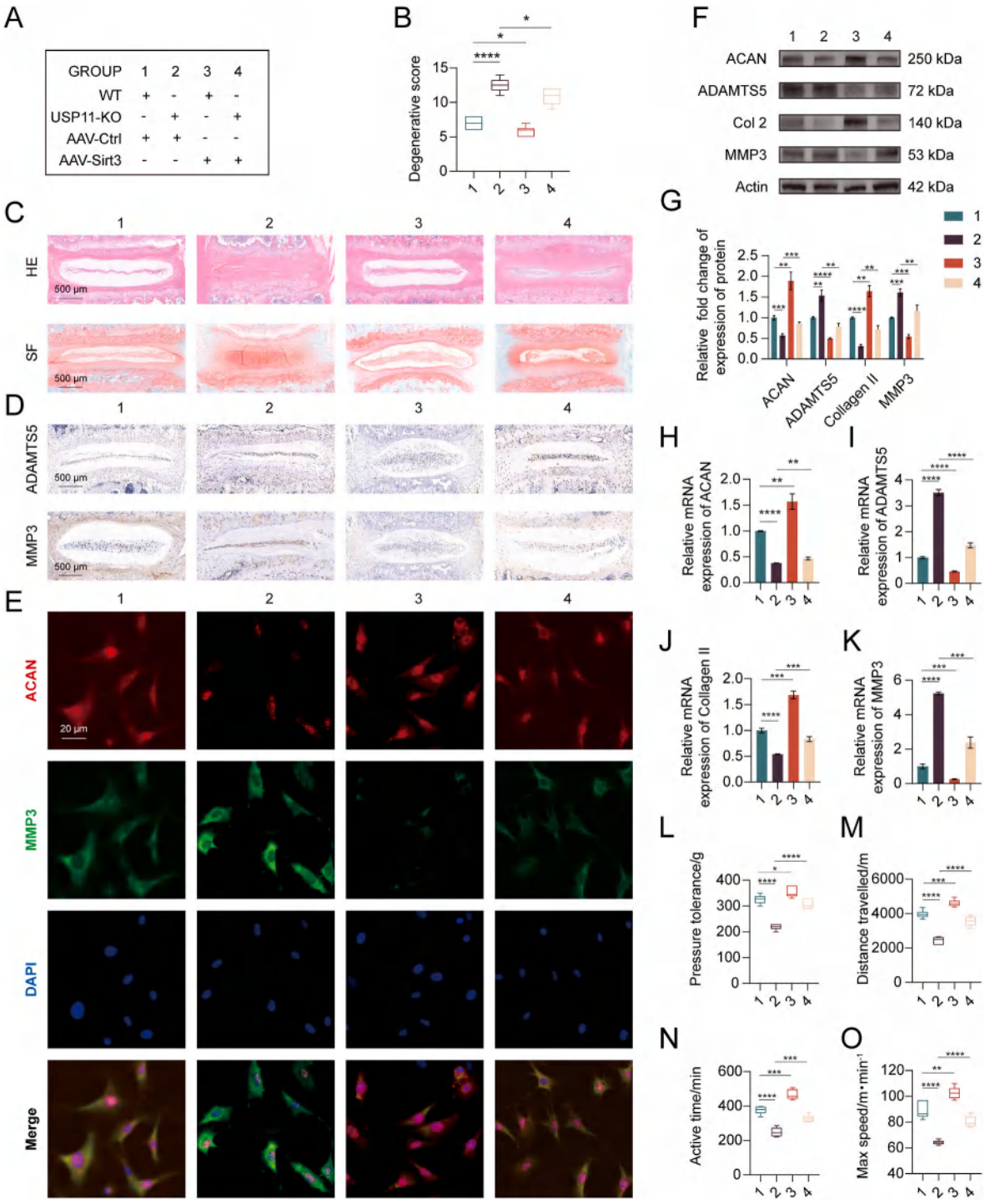

Fig. 7. (A) Detailed information of the experimental group in the part of the experiment. (B, C) KO of USP11 resulted in more severe IVDD, indicated by disrupted boundary between NP and AF tissue and decreased NP cells. (D) IHC results revealed that ADAMTS5 and MMP3 were increased significantly after KO of USP11, while AAV-Sirt3 could improve IVDD both in WT and USP11$^{-/-}$ mice. (E) KO of USP11 resulted in increased expression of MMP3 (green fluorescence) and decreased expression of ACAN (red fluorescence), which was reversed partly by AAV-Sirt3. (F, G) WB further confirmed the protective effect of AAV-Sirt3 on IVDD induced by KO of USP11. (H–K) The results above were further confirmed by qPCR. (L–O) KO of USP11 resulting in poor pain-related behavioral scores was proved, which, however, could be improved by AAV-Sirt3. * for $p < 0:05$, ** for $p < 0:01$, ***for $p < 0:001$, **** for $p < 0:0001$. (For interpretation of the references to colour in this figure legend, the reader is referred to the Web version of this article.)

mitochondrial deacetylase that promotes efficient oxidative metabolism. The involvement of Sirt3 in regulating the pathogenesis of various diseases has been reported detailly, including myocardial injury [60], osteoporosis [61], acute kidney injury [62], lymphomagenesis [63], and etc., only, however, a few researches regarding the effect of Sirt3 in IVDD have conducted. Actually, researches focusing on the effect of Sirt3 on IVDD have only emerged in recent years. In accordance with previous study [64], the current study further confirmed that Sirt3 decreased after IVDD and deletion of Sirt3 would exacerbate oxidative stress injury as expected.

PCD, such as apoptosis and autophagy as mentioned above, refers to programmed and spontaneous cell death under the gene-controlled

instructions [65]. Ferroptosis, being a newly form of PCD, has been focused by recent studies trying to elucidate the pathogenesis of IVDD. Lu et al. confirmed for the first time the involvement of ferroptosis in the process of IVDD, but only ferroportin (FPN) had been investigated in the ferroptotic event [66]. Zhang et al. further proved the involvement of ferroptosis in IVDD using single-cell RNA-seq analysis [67]. It has been reported that Sirt3 could inhibit ferroptosis in gallbladder cancer through promoting the expression of GPX4 [31,32]. Moreover, Sirt3 deficiency has been proved to be resistant to ferroptosis via deactivating SOD2/GPX4 pathway [68]. Confirmed by the current study, ferroptosis was increased with the progression of IVDD, and Sirt3 deletion exacerbated ferroptosis while ferroptosis was inhibited by overexpression of Sirt3, indicating the functional effect of Sirt3 on maintaining redox homeostasis. The crosstalk between oxidative stress and ferroptosis have been reported in serials of diseases, including ischemic stroke [30], tumors [69], acute liver failure [70]. However, the relevance of the crosstalk between oxidative stress and ferroptosis in IVDD has not been explored. In the current study, NAC, a chemical agent with thiol group that is found to be the specific oxidative stress inhibitor, was used to confirm ferroptosis was induced by oxidative stress. TBHP (an activator for oxidative stress) was proved to be responsible for ferroptosis, and compared with the treatment of TBHP, pre-treated with NAC could significantly inhibit the ferroptosis. The Sirt3 deletion was further proved to promoting oxidative stress-induced ferroptosis, while overexpression of Sirt3 inhibited ferroptosis induced by oxidative stress significantly, which implies that stabilizing and increasing the expression of Sirt3 may be a potential therapeutic method for treating IVDD. Actually, Honokiol, a small molecular weight natural compound that is able to activate Sirt3, has been reported to confer protective effect on IVDD [42,71]. However, there is still a long distance to achieve clinical administration.

There are two main ways of protein degradation in the cell: lysosomal pathway and ubiquitin-proteasome pathway [72]. Ubiquitination, one form of PTMs, refers to the process that ubiquitin (a kind of low molecular weight protein) molecules classify the proteins in the cell under the action of a series of special enzymes, select the target protein molecules from them, and make specific modifications to the target protein [73]. Most ubiquitin-labeled proteins are further transported to the proteasome for degradation [74]. DUB plays an important role in the ubiquitination pathway. In the ubiquitin-protease system, DUB cleaves the connections between the ubiquitin chains and the substrate proteins and the ubiquitin chains, so that the ubiquitin molecules can be separated from the protein substrates [75]. In the current study, we identified USP11 for the first time as the DUB that directly deubiquitinates and stabilizes Sirt3. USP11 have been reported to play a vital role in regulating neurodegenerative disorders [76], liver diseases [77], DNA damage repair [78,79], and malignant tumors [69,80]. Recently, Rong et al. have reported that USP11 plays an indispensable role in regulating iron metabolism via deubiquitinating Beclin1 that is involved in the autophagy-dependent ferroptosis [81]. In the current study, IP/MS was performed to investigate mechanism through which Sirt3 was regulated in the process of oxidative stress-induced ferroptosis, and we found that Sirt3 protein interacts with USP11 in HNP cells. Further investigations proved the direct interaction of USP11 and Sirt3 as described above. Gain and loss of function was used to prove USP11 could ameliorate ferroptosis and mitigate IVDD by increasing Sirt3 in vitro. Previous studies have showed that Sirt3 relives neuropathic pain [82,83], thus the in vivo experiments were further performed in the current study. Notably, we confirmed that USP11 depletion promotes oxidative stress-induced ferroptosis by degrading Sirt3, leading to more severe IVDD and poor pain-related behavioral scores. What accords with previous studies is that overexpression of Sirt3 could ameliorate IVDD induced by USP11 deletion [84], which indicates that the stability of Sirt3 is essential for regulatory effect of USP11 on oxidative stress-induced ferroptosis in IVDD.

In conclusion, ferroptosis is associated closely with the process of IVDD. The direct interaction of USP11 and Sirt3 is a crucial molecular event that inhibit oxidative stress-induced ferroptosis, thus improves IVDD and relives pain reaction. It may provide new methods of diagnosis and treatment for promoting NP cells survival and relieving pain after IVDD to understand the molecular mechanism of the oxidative stress-induced ferroptosis and signaling pathways of the interaction of USP11 and Sirt3 (Fig. 8). The current study has emphasized the importance of USP11-mediated de-ubiquitination of Sirt3 in HNP cells. Targeting USP11 may be a potential effective method for treating IVDD. Further studies regarding the USP11-sepecific agonists are warranted.

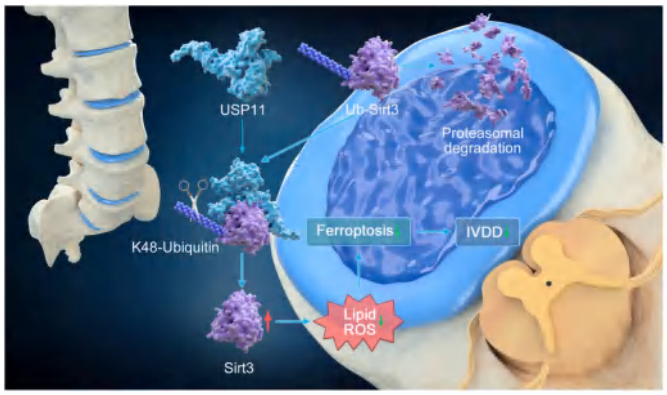

Fig. 8. USP11 regulates oxidative stress-induced ferroptosis after IVDD by deubiquitinating Sirt3. Ferroptosis is associated closely with the process of IVDD. The direct interaction of USP11 and Sirt3 is a crucial molecular event that inhibit oxidative stress-induced ferroptosis, thus improves IVDD and relives pain reaction.

Declaration of competing interest

The authors have declared that no competing interest exists.

Data availability

Data will be made available on request.

Acknowledgement

The study is supported by the National Natural Science Foundation of China, Grant/Award Numbers: No. 82172381.

Abbreviations

LBP	low back pain
IVDD	intervertebral disc degeneration
NP	nucleus pulposus
AF	annulus fibrosus
EP	endplates
PCD	programmed cell death
GSH	glutathione
ROS	reactive oxygen species
PTM	protein translational modifications
DUB	deubiquitinase
USP11	Ubiquitin specific protease 11
HNP	human nucleus pulposus
qRT-PCR	quantitative reverse transcription polymerase chain reaction
DAPI	2-(4-amidinophenyl)-1H-indole-6-carboxamidine;
MDA	malonaldehyde
Co-IP	co-immunoprecipitation
H&E	hematoxylin and eosin
S&F	safranin o & fast green

Appendix A. Supplementary data

Supplementary data to this article can be found online at https://doi.org/10.1016/j.redox.2023.102707.

References

[1] T. Morgan, J. Wu, L. Ovchinikova, R. Lindner, S. Blogg, R. Moorin, A national intervention to reduce imaging for low back pain by general practitioners: a retrospective economic program evaluation using Medicare Benefits Schedule data, BMC Health Serv. Res. 19 (2019) 983, https://doi.org/10.1186/s12913-019-4773-y.

[2] R.I. Yadav, L. Long, C. Yanming, Comparison of the effectiveness and outcome of microendoscopic and open discectomy in patients suffering from lumbar disc herniation, Medicine (Baltim.) 98 (2019), e16627, https://doi.org/10.1097/MD.0000000000016627.

[3] D. Hoy, P. Brooks, F. Blyth, R. Buchbinder, The Epidemiology of low back pain, Best Pract. Res. Clin. Rheumatol. 24 (2010) 769–781, https://doi.org/10.1016/j.berh.2010.10.002.

[4] V. Francisco, J. Pino, M.Á. González-Gay, F. Lago, J. Karppinen, O. Tervonen, A. Mobasheri, O. Gualillo, A new immunometabolic perspective of intervertebral disc degeneration, Nat. Rev. Rheumatol. 18 (2022) 47–60, https://doi.org/10.1038/s41584-021-00713-z.

[5] W. Guo, K. Mu, B. Zhang, C. Sun, L. Zhao, H.-R. Li, Z.-Y. Dong, Q. Cui, The circular RNA circ-GRB10 participates in the molecular circuitry inhibiting human intervertebral disc degeneration, Cell Death Dis. 11 (2020) 612, https://doi.org/10.1038/s41419-020-02882-3.

[6] K. Sun, J. Jiang, Y. Wang, X. Sun, J. Zhu, X. Xu, J. Sun, J. Shi, The role of nerve fibers and their neurotransmitters in regulating intervertebral disc degeneration, Ageing Res. Rev. 81 (2022), 101733, https://doi.org/10.1016/j.arr.2022.101733.

[7] Y. Zhang, B. Yang, J. Wang, F. Cheng, K. Shi, L. Ying, C. Wang, K. Xia, X. Huang, Z. Gong, C. Yu, F. Li, C. Liang, Q. Chen, Cell senescence: a nonnegligible cell state under survival stress in pathology of intervertebral disc degeneration, Oxid. Med. Cell. Longev. 2020 (2020) 1–12, https://doi.org/10.1155/2020/9503562.

[8] P.-P.A. Vergroesen, I. Kingma, K.S. Emanuel, R.J.W. Hoogendoorn, T.J. Welting, B. J. van Royen, J.H. van Dieën, T.H. Smit, Mechanics and biology in intervertebral disc degeneration: a vicious circle, Osteoarthritis Cartilage 23 (2015) 1057–1070, https://doi.org/10.1016/j.joca.2015.03.028.

[9] P.J. Roughley, Biology of intervertebral disc aging and degeneration: involvement of the extracellular matrix, Spine 29 (2004) 2691–2699, https://doi.org/10.1097/01.brs.0000146101.53784.b1.

[10] C.-Q. Zhao, L.-M. Wang, L.-S. Jiang, L.-Y. Dai, The cell biology of intervertebral disc aging and degeneration, Ageing Res. Rev. 6 (2007) 247–261, https://doi.org/10.1016/j.arr.2007.08.001.

[11] C. Weiler, In-situ-Analyse von Pathomechanismen der humanen Bandscheibendegeneration, For. Pathol. 34 (2013) 251–259, https://doi.org/10.1007/s00292-013-1813-y.

[12] J.A. Buckwalter, Aging and Degeneration of the Human Intervertebral Disc:, Spine. 20 (1995) 1307–1314, https://doi.org/10.1097/00007632-199506000-00022.

[13] K. Sun, J. Zhu, C. Yan, F. Li, F. Kong, J. Sun, X. Sun, J. Shi, Y. Wang, CGRP regulates nucleus pulposus cell apoptosis and inflammation via the MAPK/NF-κB signaling pathways during intervertebral disc degeneration, Oxid. Med. Cell. Longev. 2021 (2021) 1–19, https://doi.org/10.1155/2021/2958584.

[14] J. Zhu, K. Sun, X. Xu, J. Sun, Q. Kong, S. Wang, J. Shi, A preliminary attempt of nonintervention in the treatment of patients with intervertebral disc calcification combined with ossification of the posterior longitudinal ligament, World Neurosurg 129 (2019) 181–185, https://doi.org/10.1016/j.wneu.2019.05.169.

[15] K. Sun, J. Zhu, J. Sun, X. Sun, L. Huan, B. Zhang, F. Lin, B. Zheng, J. Jiang, X. Luo, X. Xu, J. Shi, Neuropeptide Y prevents nucleus pulposus cells from cell apoptosis and IL-1β-induced extracellular matrix degradation, Cell Cycle 20 (2021) 960–977, https://doi.org/10.1080/15384101.2021.1911914.

[16] A. Erental, Z. Kalderon, A. Saada, Y. Smith, H. Engelberg-Kulka, Apoptosis-like death, an extreme SOS response in Escherichia coli, mBio 5 (2014) e01426, https://doi.org/10.1128/mBio.01426-14, 14.

[17] M. Pasparakis, P. Vandenabeele, Necroptosis and its role in inflammation, Nature 517 (2015) 311–320, https://doi.org/10.1038/nature14191.

[18] F. Yang, Y. He, Z. Zhai, E. Sun, Programmed cell death pathways in the pathogenesis of systemic lupus erythematosus, J. Immunol. Res. 2019 (2019) 1–13, https://doi.org/10.1155/2019/3638562.

[19] J. Tower, Programmed cell death in aging, Ageing Res. Rev. 23 (2015) 90–100, https://doi.org/10.1016/j.arr.2015.04.002.

[20] S.-K. Hsu, C.-Y. Li, I.-L. Lin, W.-J. Syue, Y.-F. Chen, K.-C. Cheng, Y.-N. Teng, Y.-H. Lin, C.-H. Yen, C.-C. Chiu, Inflammation-related pyroptosis, a novel programmed cell death pathway, and its crosstalk with immune therapy in cancer treatment, Theranostics 11 (2021) 8813–8835, https://doi.org/10.7150/thno.62521.

[21] X. Chen, J. Li, R. Kang, D.J. Klionsky, D. Tang, Ferroptosis: machinery and regulation, Autophagy 17 (2021) 2054–2081, https://doi.org/10.1080/15548627.2020.1810918.

[22] S.J. Dixon, K.M. Lemberg, M.R. Lamprecht, R. Skouta, E.M. Zaitsev, C.E. Gleason, D.N. Patel, A.J. Bauer, A.M. Cantley, W.S. Yang, B. Morrison, B.R. Stockwell, Ferroptosis: an iron-dependent form of nonapoptotic cell death, Cell 149 (2012) 1060–1072, https://doi.org/10.1016/j.cell.2012.03.042.

[23] T. Hirschhorn, B.R. Stockwell, The development of the concept of ferroptosis, Free Radic. Biol. Med. 133 (2019) 130–143, https://doi.org/10.1016/j.freeradbiomed.2018.09.043.

[24] Y. Mou, J. Wang, J. Wu, D. He, C. Zhang, C. Duan, B. Li, Ferroptosis, a new form of cell death: opportunities and challenges in cancer, J. Hematol. Oncol.J Hematol Oncol. 12 (2019) 34, https://doi.org/10.1186/s13045-019-0720-y.

[25] Y. Tian, J. Lu, X. Hao, H. Li, G. Zhang, X. Liu, X. Li, C. Zhao, W. Kuang, D. Chen, M. Zhu, FTH1 inhibits ferroptosis through ferritinophagy in the 6-OHDA model of Parkinson's disease, Neurotherapeutics 17 (2020) 1796–1812, https://doi.org/10.1007/s13311-020-00929-z.

[26] M. Jia, D. Qin, C. Zhao, L. Chai, Z. Yu, W. Wang, L. Tong, L. Lv, Y. Wang, J. Rehwinkel, J. Yu, W. Zhao, Redox homeostasis maintained by GPX4 facilitates STING activation, Nat. Immunol. 21 (2020) 727–735, https://doi.org/10.1038/s41590-020-0699-0.

[27] S. Doll, B. Proneth, Y.Y. Tyurina, E. Panzilius, S. Kobayashi, I. Ingold, M. Irmler, J. Beckers, M. Aichler, A. Walch, H. Prokisch, D. Trümbach, G. Mao, F. Qu, H. Bayir, J. Füllekrug, C.H. Scheel, W. Wurst, J.A. Schick, V.E. Kagan, J.P.F. Angeli, M. Conrad, ACSL4 dictates ferroptosis sensitivity by shaping cellular lipid composition, Nat. Chem. Biol. 13 (2017) 91–98, https://doi.org/10.1038/nchembio.2239.

[28] Y. Zhou, H. Zhou, L. Hua, C. Hou, Q. Jia, J. Chen, S. Zhang, Y. Wang, S. He, E. Jia, Verification of ferroptosis and pyroptosis and identification of PTGS2 as the hub gene in human coronary artery atherosclerosis, Free Radic, Biol. Med. 171 (2021) 55–68, https://doi.org/10.1016/j.freeradbiomed.2021.05.009.

[29] M.W. Park, H.W. Cha, J. Kim, J.H. Kim, H. Yang, S. Yoon, N. Boonpraman, S.S. Yi, I.D. Yoo, J.-S. Moon, NOX4 promotes ferroptosis of astrocytes by oxidative stress-induced lipid peroxidation via the impairment of mitochondrial metabolism in Alzheimer's diseases, Redox Biol. 41 (2021), 101947, https://doi.org/10.1016/j.redox.2021.101947.

[30] J.-X. Ren, C. Li, X.-L. Yan, Y. Qu, Y. Yang, Z.-N. Guo, Crosstalk between oxidative stress and ferroptosis/oxytosis in ischemic stroke: possible targets and molecular mechanisms, Oxid. Med. Cell. Longev. 2021 (2021) 1–13, https://doi.org/10.1155/2021/6643382.

[31] D. Han, L. Jiang, X. Gu, S. Huang, J. Pang, Y. Wu, J. Yin, J. Wang, SIRT3 deficiency is resistant to autophagy-dependent ferroptosis by inhibiting the AMPK/mTOR pathway and promoting GPX4 levels, J. Cell. Physiol. 235 (2020) 8839–8851, https://doi.org/10.1002/jcp.29727.

[32] L. Liu, Y. Li, D. Cao, S. Qiu, Y. Li, C. Jiang, R. Bian, Y. Yang, L. Li, X. Li, Z. Wang, Z. Ju, Y. Zhang, Y. Liu, SIRT3 inhibits gallbladder cancer by induction of AKT-dependent ferroptosis and blockade of epithelial-mesenchymal transition, Cancer Lett. 510 (2021) 93–104, https://doi.org/10.1016/j.canlet.2021.04.007.

[33] J. Lin, J. Du, X. Wu, C. Xu, J. Liu, L. Jiang, X. Cheng, G. Ge, L. Chen, Q. Pang, D. Geng, H. Mao, SIRT3 mitigates intervertebral disc degeneration by delaying oxidative stress-induced senescence of nucleus pulposus cells, J. Cell. Physiol. 236 (2021) 6441–6456, https://doi.org/10.1002/jcp.30319.

[34] G.-Z. Zhang, Y.-J. Deng, Q.-Q. Xie, E.-H. Ren, Z.-J. Ma, X.-G. He, Y.-C. Gao, X.-W. Kang, Sirtuins and intervertebral disc degeneration: roles in inflammation, oxidative stress, and mitochondrial function, Clin. Chim. Acta 508 (2020) 33–42, https://doi.org/10.1016/j.cca.2020.04.016.

[35] T.-Y. Zhou, Y.-G. Wu, Y.-Z. Zhang, Y.-W. Bao, Y. Zhao, SIRT3 retards intervertebral disc degeneration by anti-oxidative stress by activating the SIRT3/FOXO3/SOD2 signaling pathway, Eur. Rev. Med. Pharmacol. Sci. 23 (2019) 9180–9188, https://doi.org/10.26355/eurrev_201911_19408.

[36] W. Critchley, C. Pellet-Many, B. Ringham-Terry, M. Harrison, I. Zachary, S. Ponnambalam, Receptor tyrosine kinase ubiquitination and de-ubiquitination in signal transduction and receptor trafficking, Cells 7 (2018) 22, https://doi.org/10.3390/cells7030022.

[37] H. Sun, B. Ou, S. Zhao, X. Liu, L. Song, X. Liu, R. Wang, Z. Peng, USP11 promotes growth and metastasis of colorectal cancer via PPP1CA-mediated activation of ERK/MAPK signaling pathway, EBioMedicine 48 (2019) 236–247, https://doi.org/10.1016/j.ebiom.2019.08.061.

[38] X. Zhu, Y. Zhang, Q. Luo, X. Wu, F. Huang, T. Shu, Y. Wan, H. Chen, Z. Liu, The deubiquitinase USP11 promotes ovarian cancer chemoresistance by stabilizing BIP, Signal Transduct. Targeted Ther. 6 (2021) 264, https://doi.org/10.1038/s41392-021-00580-w.

[39] C. Meng, J. Zhan, D. Chen, G. Shao, H. Zhang, W. Gu, J. Luo, The deubiquitinase USP11 regulates cell proliferation and ferroptotic cell death via stabilization of NRF2 USP11 deubiquitinates and stabilizes NRF2, Oncogene 40 (2021) 1706–1720, https://doi.org/10.1038/s41388-021-01660-5.

[40] X. Zhang, T. Liu, S. Xu, P. Gao, W. Dong, W. Liu, M. Gao, L. Song, L. Cui, X. Dong, A pro-inflammatory mediator USP11 enhances the stability of p53 and inhibits KLF2 in intracerebral hemorrhage, Mol. Ther. - Methods Clin. Dev. 21 (2021) 681–692, https://doi.org/10.1016/j.omtm.2021.01.015.

[41] K. Sun, J. Zhu, Y. Deng, X. Xu, F. Kong, X. Sun, L. Huan, C. Ren, J. Sun, J. Shi, Gamabufotalin inhibits osteoclastgenesis and counteracts estrogen-deficient bone loss in mice by suppressing RANKL-induced NF-κB and ERK/MAPK pathways, Front. Pharmacol. 12 (2021), 629968, https://doi.org/10.3389/fphar.2021.629968.

[42] X. Huang, H. Shu, C. Ren, J. Zhu, SIRT3 improves bone regeneration and rescues diabetic fracture healing by regulating oxidative stress, Biochem. Biophys. Res. Commun. 604 (2022) 109–115, https://doi.org/10.1016/j.bbrc.2022.03.001.

[43] L. Xie, W. Huang, Z. Fang, F. Ding, F. Zou, X. Ma, J. Tao, J. Guo, X. Xia, H. Wang, Z. Yu, F. Lu, J. Jiang, CircERCC2 ameliorated intervertebral disc degeneration by regulating mitophagy and apoptosis through miR-182-5p/SIRT1 axis, Cell Death Dis. 10 (2019) 751, https://doi.org/10.1038/s41419-019-1978-2.

[44] T.D. Wiltshire, C.A. Lovejoy, T. Wang, F. Xia, M.J. O'Connor, D. Cortez, Sensitivity to poly(ADP-ribose) polymerase (PARP) inhibition identifies ubiquitin-specific peptidase 11 (USP11) as a regulator of DNA double-strand break repair, J. Biol. Chem. 285 (2010) 14565–14571, https://doi.org/10.1074/jbc.M110.104745.
[45] E.-W. Lee, D. Seong, J. Seo, M. Jeong, H.-K. Lee, J. Song, USP11-dependent selective cIAP2 deubiquitylation and stabilization determine sensitivity to Smac mimetics, Cell Death Differ. 22 (2015) 1463–1476, https://doi.org/10.1038/cdd.2014.234.
[46] M. Jurga, A.A. Abugable, A.S.H. Goldman, S.F. El-Khamisy, USP11 controls R-loops by regulating senataxin proteostasis, Nat. Commun. 12 (2021) 5156, https://doi.org/10.1038/s41467-021-25459-w.
[47] L. Feng, C. Li, L.-W. Zeng, D. Gao, Y.-H. Sun, L. Zhong, H. Lin, H.-B. Shu, S. Li, MARCH3 negatively regulates IL-3-triggered inflammatory response by mediating K48-linked polyubiquitination and degradation of IL-3Rα, Signal Transduct. Targeted Ther. 7 (2022) 21, https://doi.org/10.1038/s41392-021-00834-7.
[48] Y.-T. Wang, T.-Y. Liu, C.-H. Shen, S.-Y. Lin, C.-C. Hung, L.-C. Hsu, G.-C. Chen, K48/K63-linked polyubiquitination of ATG9A by TRAF6 E3 ligase regulates oxidative stress-induced autophagy, Cell Rep. 38 (2022), 110354, https://doi.org/10.1016/j.celrep.2022.110354.
[49] G. Zhu, M. Herlyn, X. Yang, TRIM15 and CYLD regulate ERK activation via lysine-63-linked polyubiquitination, Nat. Cell Biol. 23 (2021) 978–991, https://doi.org/10.1038/s41556-021-00732-8.
[50] Y. Wang, Q. Zhan, X. Wang, P. Li, S. Liu, G. Gao, P. Gao, Insights into catalysis and regulation of non-canonical ubiquitination and deubiquitination by bacterial deamidase effectors, Nat. Commun. 11 (2020) 2751, https://doi.org/10.1038/s41467-020-16587-w.
[51] K. Arimoto, K. Funami, Y. Saeki, K. Tanaka, K. Okawa, O. Takeuchi, S. Akira, Y. Murakami, K. Shimotohno, Polyubiquitin conjugation to NEMO by triparite motif protein 23 (TRIM23) is critical in antiviral defense, Proc. Natl. Acad. Sci. USA 107 (2010) 15856–15861, https://doi.org/10.1073/pnas.1004621107.
[52] M. Harreman, M. Taschner, S. Sigurdsson, R. Anindya, J. Reid, B. Somesh, S. E. Kong, C.A.S. Banks, R.C. Conaway, J.W. Conaway, J.Q. Svejstrup, Distinct ubiquitin ligases act sequentially for RNA polymerase II polyubiquitylation, Proc. Natl. Acad. Sci. USA 106 (2009) 20705–20710, https://doi.org/10.1073/pnas.0907052106.
[53] N. Kos, L. Gradisnik, T. Velnar, A brief review of the degenerative intervertebral disc disease, Med. Arch. 73 (2019) 421, https://doi.org/10.5455/medarh.2019.73.421-424.
[54] Z. Tang, B. Hu, F. Zang, J. Wang, X. Zhang, H. Chen, Nrf2 drives oxidative stress-induced autophagy in nucleus pulposus cells via a Keap1/Nrf2/p62 feedback loop to protect intervertebral disc from degeneration, Cell Death Dis. 10 (2019) 510, https://doi.org/10.1038/s41419-019-1701-3.
[55] F. Cornaz, J. Widmer, N.A. Farshad-Amacker, J.M. Spirig, J.G. Snedeker, M. Farshad, Intervertebral disc degeneration relates to biomechanical changes of spinal ligaments, Spine J. 21 (2021) 1399–1407, https://doi.org/10.1016/j.spinee.2021.04.016.
[56] D. Chen, D. Xia, Z. Pan, D. Xu, Y. Zhou, Y. Wu, N. Cai, Q. Tang, C. Wang, M. Yan, J. J. Zhang, K. Zhou, Q. Wang, Y. Feng, X. Wang, H. Xu, X. Zhang, N. Tian, Metformin protects against apoptosis and senescence in nucleus pulposus cells and ameliorates disc degeneration in vivo, Cell Death Dis. 7 (2016), https://doi.org/10.1038/cddis.2016.334 e2441–e2441.
[57] C.-Q. Zhao, Y.-H. Zhang, S.-D. Jiang, L.-S. Jiang, L.-Y. Dai, Both endoplasmic reticulum and mitochondria are involved in disc cell apoptosis and intervertebral disc degeneration in rats, Age 32 (2010) 161–177, https://doi.org/10.1007/s11357-009-9121-4.
[58] F.J. Blanco, I. Rego, C. Ruiz-Romero, The role of mitochondria in osteoarthritis, Nat. Rev. Rheumatol. 7 (2011) 161–169, https://doi.org/10.1038/nrrheum.2010.213.
[59] L.D. Osellame, M.R. Duchen, Quality control gone wrong: mitochondria, lysosomal storage disorders and neurodegeneration, Br. J. Pharmacol. 171 (2014) 1958–1972, https://doi.org/10.1111/bph.12453.
[60] T. Xin, C. Lu, SirT3 activates AMPK-related mitochondrial biogenesis and ameliorates sepsis-induced myocardial injury, Aging 12 (2020) 16224–16237, https://doi.org/10.18632/aging.103644.
[61] Y. Guo, X. Jia, Y. Cui, Y. Song, S. Wang, Y. Geng, R. Li, W. Gao, D. Fu, Sirt3-mediated mitophagy regulates AGEs-induced BMSCs senescence and senile osteoporosis, Redox Biol. 41 (2021), 101915, https://doi.org/10.1016/j.redox.2021.101915.
[62] A. Khanna Anamika, P. Acharjee, A. Acharjee, S.K. Trigun, Mitochondrial SIRT3 and neurodegenerative brain disorders, J. Chem. Neuroanat. 95 (2019) 43–53, https://doi.org/10.1016/j.jchemneu.2017.11.009.
[63] M. Li, Y.-L. Chiang, C.A. Lyssiotis, M.R. Teater, J.Y. Hong, H. Shen, L. Wang, J. Hu, H. Jing, Z. Chen, N. Jain, C. Duy, S.J. Mistry, L. Cerchietti, J.R. Cross, L.C. Cantley, M.R. Green, H. Lin, A.M. Melnick, Non-oncogene addiction to SIRT3 plays a critical role in lymphomagenesis, Cancer Cell 35 (2019) 916–931.e9, https://doi.org/10.1016/j.ccell.2019.05.002.
[64] S. Hu, C. Zhang, T. Qian, Y. Bai, L. Chen, J. Chen, C. Huang, C. Xie, X. Wang, H. Jin, Promoting nrf2/sirt3-dependent mitophagy suppresses apoptosis in nucleus pulposus cells and protects against intervertebral disc degeneration, Oxid. Med. Cell. Longev. 2021 (2021) 1–20, https://doi.org/10.1155/2021/6694964.
[65] G.S. Kopeina, B. Zhivotovsky, Programmed cell death: past, present and future, Biochem. Biophys. Res. Commun. 633 (2022) 55–58, https://doi.org/10.1016/j.bbrc.2022.09.022.
[66] S. Lu, Y. Song, R. Luo, S. Li, G. Li, K. Wang, Z. Liao, B. Wang, W. Ke, Q. Xiang, C. Chen, X. Wu, Y. Zhang, L. Ling, C. Yang, Ferroportin-dependent iron homeostasis protects against oxidative stress-induced nucleus pulposus cell ferroptosis and ameliorates intervertebral disc degeneration in vivo, Oxid. Med. Cell. Longev. 2021 (2021) 1–18, https://doi.org/10.1155/2021/6670497.
[67] Y. Zhang, S. Han, M. Kong, Q. Tu, L. Zhang, X. Ma, Single-cell RNA-seq analysis identifies unique chondrocyte subsets and reveals involvement of ferroptosis in human intervertebral disc degeneration, Osteoarthritis Cartilage 29 (2021) 1324–1334, https://doi.org/10.1016/j.joca.2021.06.010.
[68] Q. Li, J. Liao, W. Chen, K. Zhang, H. Li, F. Ma, H. Zhang, Q. Han, J. Guo, Y. Li, L. Hu, J. Pan, Z. Tang, NAC alleviative ferroptosis in diabetic nephropathy via maintaining mitochondrial redox homeostasis through activating SIRT3-SOD2/Gpx4 pathway, Free Radic. Biol. Med. 187 (2022) 158–170, https://doi.org/10.1016/j.freeradbiomed.2022.05.024.
[69] J. Zhu, Y. Xiong, Y. Zhang, J. Wen, N. Cai, K. Cheng, H. Liang, W. Zhang, The molecular mechanisms of regulating oxidative stress-induced ferroptosis and therapeutic strategy in tumors, Oxid. Med. Cell. Longev. 2020 (2020) 1–14, https://doi.org/10.1155/2020/8810785.
[70] Y. Wang, Q. Chen, C. Shi, F. Jiao, Z. Gong, Mechanism of glycyrrhizin on ferroptosis during acute liver failure by inhibiting oxidative stress, Mol. Med. Rep. (2019), https://doi.org/10.3892/mmr.2019.10660.
[71] J. Wang, M. Nisar, C. Huang, X. Pan, D. Lin, G. Zheng, H. Jin, D. Chen, N. Tian, Q. Huang, Y. Duan, Y. Yan, K. Wang, C. Wu, J. Hu, X. Zhang, X. Wang, Small molecule natural compound agonist of SIRT3 as a therapeutic target for the treatment of intervertebral disc degeneration, Exp. Mol. Med. 50 (2018) 1–14, https://doi.org/10.1038/s12276-018-0173-3.
[72] A. Hanzl, G.E. Winter, Targeted protein degradation: current and future challenges, Curr. Opin. Chem. Biol. 56 (2020) 35–41, https://doi.org/10.1016/j.cbpa.2019.11.012.
[73] D. Popovic, D. Vucic, I. Dikic, Ubiquitination in disease pathogenesis and treatment, Nat. Med. 20 (2014) 1242–1253, https://doi.org/10.1038/nm.3739.
[74] N. Nakamura, Ubiquitin system, Int. J. Mol. Sci. 19 (2018) 1080, https://doi.org/10.3390/ijms19041080.
[75] N.J. Schauer, R.S. Magin, X. Liu, L.M. Doherty, S.J. Buhrlage, Advances in discovering deubiquitinating enzyme (DUB) inhibitors, J. Med. Chem. 63 (2020) 2731–2750, https://doi.org/10.1021/acs.jmedchem.9b01138.
[76] S.-Y. Chiang, H.-C. Wu, S.-Y. Lin, H.-Y. Chen, C.-F. Wang, N.-H. Yeh, J.-H. Shih, Y.-S. Huang, H.-C. Kuo, S.-J. Chou, R.-H. Chen, Usp11 controls cortical neurogenesis and neuronal migration through Sox11 stabilization, Sci. Adv. 7 (2021), eabc6093, https://doi.org/10.1126/sciadv.abc6093.
[77] H. Yang, D. Park, J. Ryu, T. Park, USP11 degrades KLF4 via its deubiquitinase activity in liver diseases, J. Cell Mol. Med. 25 (2021) 6976–6987, https://doi.org/10.1111/jcmm.16709.
[78] T. Deng, G. Yan, X. Song, L. Xie, Y. Zhou, J. Li, X. Hu, Z. Li, J. Hu, Y. Zhang, H. Zhang, Y. Sun, P. Feng, D. Wei, B. Hu, J. Liu, W. Tan, M. Ye, Deubiquitylation and stabilization of p21 by USP11 is critical for cell-cycle progression and DNA damage responses, Proc. Natl. Acad. Sci. USA 115 (2018) 4678–4683, https://doi.org/10.1073/pnas.1714938115.
[79] X. Ting, L. Xia, J. Yang, L. He, W. Si, Y. Shang, L. Sun, USP11 acts as a histone deubiquitinase functioning in chromatin reorganization during DNA repair, Nucleic Acids Res. 47 (2019) 9721–9740, https://doi.org/10.1093/nar/gkz726.
[80] L. Dwane, A.E. O'Connor, S. Das, B. Moran, L. Mulrane, A. Pinto-Fernandez, E. Ward, A.M. Blümel, B.L. Cavanagh, B. Mooney, A.M. Dirac, K. Jirström, B. M. Kessler, T. Ní Chonghaile, R. Bernards, W.M. Gallagher, D.P. O'Connor, A functional genomic screen identifies the deubiquitinase USP11 as a novel transcriptional regulator of ERα in breast cancer, Cancer Res. 80 (2020) 5076–5088, https://doi.org/10.1158/0008-5472.CAN-20-0214.
[81] Y. Rong, J. Fan, C. Ji, Z. Wang, X. Ge, J. Wang, W. Ye, G. Yin, W. Cai, W. Liu, USP11 regulates autophagy-dependent ferroptosis after spinal cord ischemia-reperfusion injury by deubiquitinating Beclin 1, Cell Death Differ. 29 (2022) 1164–1175, https://doi.org/10.1038/s41418-021-00907-8.
[82] B. Yan, Q. Liu, X. Ding, Y. Lin, X. Jiao, Y. Wu, H. Miao, C. Zhou, SIRT3-Mediated CypD-K166 deacetylation alleviates neuropathic pain by improving mitochondrial dysfunction and inhibiting oxidative stress, Oxid. Med. Cell. Longev. 2022 (2022) 1–17, https://doi.org/10.1155/2022/4722647.
[83] C. Zhou, Y. Zhang, X. Jiao, G. Wang, R. Wang, Y. Wu, SIRT3 alleviates neuropathic pain by deacetylating FoxO3a in the spinal dorsal horn of diabetic model rats, Reg. Anesth. Pain Med. 46 (2021) 49–56, https://doi.org/10.1136/rapm-2020-101918.
[84] B. Hu, P. Wang, S. Zhang, W. Liu, X. Lv, D. Shi, L. Zhao, H. Liu, B. Wang, S. Chen, Z. Shao, HSP70 attenuates compression-induced apoptosis of nucleus pulposus cells by suppressing mitochondrial fission via upregulating the expression of SIRT3, Exp. Mol. Med. 54 (2022) 309–323, https://doi.org/10.1038/s12276-022-00745-9.